1-1-2017

Engineering Crystallization Via Phase Field Crystal Model

Deepak Joshi
Wayne State University,

ENGINEERING CRYSTALLIZATION via PHASE FIELD CRYSTAL MODEL

by

DEEPAK JOSHI

THESIS

Submitted to the Graduate School

of Wayne State University,

Detroit, Michigan

in partial fulfilment of the requirements

for the degree of

MASTER OF SCIENCE

2017

MAJOR: MATERIALS SCIENCE AND ENGINEERING

Approved By:

Advisor Date

ACKNOWLEDGMENTS

I express my deep and sincere sense of indebtedness to my guide my guide Dr Korosh Torabi**,** Asst Professor Department of Chemical and Materials engineering, Wayne State University, Detroit, Michigan, United States for his invaluable guidance, painstaking effort thorough each and every step of my project work throughout the year.

I am thankful to my co guide Dr Guangzhao Mao, Chair Professor, Chemical and Materials Engineering, Wayne State University for letting me access her lab facilities for carrying experimental part of this thesis.

Last but not the least I would like to thanks my Lab members, friends and family members for being a constant source of encouragement throughout the year.

Deepak Joshi

Table of Contents

List of Figures

Chapter I- Research objective

The primary objective of the undertaken work is to study the effect of external parameters such as the substrate nature, solute concentration, over-potential on the electro crystallization of charge transfer complex organic nanorod of TTF (tetrathiafulvalene) and TCNQ(7,7,8,8,-tetracyanoquinodimethane) on a substrate[1]. The basis of this work is the analogy which assumes that control of these parameters governs the final morphology of the electro crystallized nanorods which in turn is necessary regarding their integration as nanomaterials and nanodevices for patterned circuitry. Moreover, we have prescribed an additional analogy that the change in solute concentration and applied overpotential have a net effect in rendering the electro crystallization process as preferably thermodynamically or kinetically driven. The proposed research objective sought to be achieved by the justification of the obtained experimental evidences with a theoretical model.

On the theoretical front the process is considered in line with a Classical Density Functional Theory-CDFT model which initializes the thermodynamic state of the system in terms of Helmholtz free energy functional of one particle density[2–4].

We did perform initial analysis of the experimental results which paved our way towards Phase field crystal model built up on the very concepts of CDFT. The derivation of PFC model comes through after approximation to the model of Classical density functional theory. We have performed an in-depth review of the work where PFC model has been applied extensively to study crystallization and thus have resort to the model for our theoretical study.

Chapter II-Introduction and Background research

II-I Classical Density Functional Theory

The CDFT model is built up on the concepts of Classical thermodynamics and Statistical mechanics. In mathematical terms the model consider the system in terms of Helmholtz free energy functional of one particle density. The Helmholtz free energy functional is represented as[2,5]:

$$F[\rho] = F_{idl}[\rho] + F_{exc}[\rho] \qquad (1)$$

, where $F_{idl}[\rho]$ represents free energy as that of an ideal gas given by:

$$F_{idl} = kT \int dr\rho(r)[ln\Lambda^3\rho(r) - 1] \qquad (2)$$

and $\Lambda=\frac{h}{\sqrt{2\pi mkT}}$is the de Broglie wavelength, m is the mass of particles, h is the Plank's constant, k is the Boltzmann constant and T is the temperature

Whereas, the one particle density is denoted as an ensemble average[2]

$$\rho(r) = \langle \sum \delta(r - r_i) \rangle \qquad (3)$$

, where r_i is the position of a particle/atom in a system

Finally, the second term in the Helmholtz free energy equation accounts for the interaction between the particle in the system. There is no exact expression for $F_{exc}[\rho]$ and because of which one must resort to various approximate approaches for its evaluation. One of such approximation involves the expansion of the excess Helmholtz free energy functional $F_{exc}(\rho)$ in a Taylor series around the density of reference fluid till the second order[6]. One of the other known approximation in this direction is the fundamental measure theory or the weighted density approximation given by Rosenfield proposed specifically for

a system of hard spheres[3].The theory suggest the excess free energy functional can be taken as a combination of weighted densities, which can be written as[3]:

$$F[(\rho_i)] = \int dr\Phi\{n_v(r)\} \qquad (4)$$

, where Φ is the excess free energy density as a function of n_v , the weighted density. The weighted density has scalar and vector component which depends upon m number of weight scaling factor (w_i) used. They are written as[3]:

$$n_v(r) = \sum_{i=1}^{m} \int dr' \rho_i(r') w(r - r') = \sum_{i=1}^{m} (\rho_i * w_v^i) \qquad (5)$$

, where ρ_i denotes the density distribution of species i and w_v^i denotes the weight functions having the scalar and vector components. Another approach that leads to the calculation of the excess free energy functional is the Mean field approach where the interaction are composed of soft or ultra-soft interaction [7] like Lennard Jones .In this case the excess free energy functional is written as[5]:

$$F_{exc} = \frac{1}{2} \iint dr dr' \rho(r) \rho(r') \varphi(|r - r'|) \qquad (6)$$

All thermodynamics state of the system is related to the grand canonical potential which is related to the Helmholtz free energy[2]:

$$\Omega(r) = F(\rho) - \mu \int \rho(r) dr \qquad (7)$$

, where μ is the imposed chemical potential.

Thus, in a CDFT model the equilibrium criteria is based upon finding out that one particle density configuration $\rho_0(r)$ which minimizes the grand canonical potential. In Mathematical terms the following equation reflects the minimization criteria[2]:

$$\frac{\delta\Omega[\rho]}{\delta\rho} = 0, or \ \frac{\delta F[\rho]}{\delta\rho} - \mu = 0 \qquad (8)$$

In the next section we will introduce an extension of Density Functional theory to time domain known as the Dynamical Density Functional Theory(DDFT model).In the DDFT model the time evolution of the ensemble average of particle position inside a system is given by an integro-differential equation in terms of the equilibrium Helmholtz free energy functional(or the grand canonical function).The time evolution of one particle density can be understood in terms of relaxation dynamics between the particle and the surrounding fluid as the system moves towards an equilibrium state.

II-2 Dynamical Density Functional theory (DDFT)

The need to study the time evolution of one particle density ρ(r, t) in a non-equilibrium fluid lead to the development of Dynamical Density Functional theory [8]derived from the fundamentals of CDFT. To derive the DDFT model one needs to look at the Langevian equation which considers the motion of N particles under the influence of internal and external force. The force between the particles is caused by the net acting potential given by[5]:

$$U = U_{ext} + U_{int} \qquad (9)$$

, where $U_{ext}(r_1, r_2 \dots r_N) = \sum U_1(r_i, t)$ and $U_{int} = \sum U_2(r_i - r_j)$

The expression of N particle density is given by Smoluchowsk equation in terms of N particle probability density distribution[9]

$$\frac{dP(r1,r2\dots rN)}{dt} = \hat{L}\, P(r_1, r_2 \dots r_N) \qquad (10)$$

with the Smoluchowski operator given as[5,9]

$$\hat{L} = D \sum \nabla_{r_i} \left(\nabla_{r_i} \frac{U(r_1,r_2\dots r_N)}{kT} + \nabla_{r_i} \right) \qquad (11)$$

In general, the n particle density ρ^n (n<N) distribution is directly proportional to the n particle probability density P ($r_1, r_2 \ldots r_N$) density as[5]:

$$\rho^n(r_1, r_2 \ldots r_N) = \frac{N!}{(N-n)!} \int dr_{N+1} \int \int \ldots . \int dr_N P(r_1, r_2 \ldots r_N) \qquad (12)$$

Now integrating Smoluchowski equation (10) over (N-1) particle position and combining it with the equation (12) and (11) we get the one particle density variation with time

$$\frac{d\rho(r,t)}{dt} = D\nabla_r . \left[\nabla_r \rho(r,t) - \frac{f(r,t)}{kT} + \frac{\rho(r,t)}{kT} \nabla_r U_1(r,t)\right] \qquad (13)$$

, where $f(r,t) = -\int dr' \, \rho^2(r,r',t) \nabla_r U(|r-r'|)$

As discussed in previous section the Helmholtz free energy functional is sometimes approximated by a mean field approach as [2,5] given by equation (6)

$$F_{exc} = \frac{1}{2} \int \int dr dr' \rho(r) \rho(r') U_2(|r-r'|)$$

Correlating to the above expression of excess Helmholtz free energy f(r,t) can be written as [5]

$$f(r,t) = -\rho(r) \nabla_r \frac{\delta F_{exc}[\rho(r,t)]}{\delta \rho(r,t)} \qquad (14)$$

$$\text{Also } \nabla_r U_1(r,t) = \nabla_r \frac{\delta F_{ext}[\rho(r,t)]}{\delta \rho(r,t)} \qquad (15),$$

$$\nabla_r \rho(r,t) = \frac{1}{kT} \times \rho(r,t) \nabla_r \frac{\delta F_{id}[\rho(r,t)]}{\delta \rho(r,t)} \qquad (16)$$

,where $F_{idl} = kT \int dr \rho(r) [ln\wedge^3 \rho(r) - 1]$ and $F_{ext} = \int dr \rho(r) V_{ext}(r)$ .Besides the expression $\frac{\delta F_{id}[\rho(r,t)]}{\delta \rho(r,t)}$, $\frac{\delta F_{ext}[\rho(r,t)]}{\delta \rho(r,t)}$, $\frac{\delta F_{exc}[\rho(r,t)]}{\delta \rho(r,t)}$ are the functional derivative of ideal

,external and excess Helmholtz free energy with respect to one particle density and ∇_r is the gradient operation on these expression in space variable r.

Incorporating (14), (15) and (16) together in (13) we come to the fundamental equation of Dynamical density functional theory[5].

$$\frac{d\rho(r,t)}{dt} = \frac{D}{kT}\nabla_r.\left[\rho(r,t)\nabla_r\frac{\delta F[\rho(r,t)]}{\delta\rho(r,t)}\right]$$

For time-independent external potentials V_{ext}(r) the DDFT describes the relaxation dynamics of the density field toward equilibrium at the minimum of the Helmholtz free-energy functional $F[\rho_0]$, given an exact canonical excess free-energy functional $F_{exc}[\rho]$.

II-3 Phase Field Crystal Model (PFC)

Similar to a DDFT model the phase field crystal model consider the system in terms of Helmholtz free energy functional Ƒ [Ψ (r, t)] of a phase field Ψ (r, t). The phase field model can be derived by taking into account the expansion of the free energy Helmholtz free energy functional around a density of a reference liquid as was proposed[6] by Ramakrishnan-Yussouff.

The final derived equation which represents the PFC model contain terms which are dimensionless in nature and represents the physical attributes of fluids and crystals [10,11].The derivation of PFC model follows up from the expansion of the difference in Helmholtz free energy $\Delta F=F-F_{ref}$ functional between the crystal and reference fluid (ρ_L^{ref})density difference $\Delta\rho = \rho - \rho_L^{ref}$ in the following manner[12].

$F[\rho] = F\left[\rho_L^{ref}\right] + \int \frac{\delta F[\rho]}{\delta\rho(r)}|_{\rho_0}\,\Delta\rho(r)dr + \frac{1}{2}\int\int \frac{\delta F[\rho]}{\delta\rho(r1)\delta(r2)}|_{\rho_0}\,\Delta\rho(r1)\Delta\rho(r2))dr1dr2$ +Ideal free energy. Truncating the Taylor expansion to two terms[11]

$$\frac{\Delta F}{k_B T} = \int dr\left[(\rho\ln\left(\frac{\rho}{\rho_L^{ref}}\right) - \Delta\rho\right] - \frac{1}{2}\iint dr_1 dr_2\Delta\rho(r1)\Delta\rho(r2) * C(|r1-r2|) \qquad (17)$$

, where $C(|r_1 - r_2|)$ is equal to $\frac{\delta F[\rho]}{\delta\rho(r1)\delta\rho(r2)}$ in the above equation.

The equilibrium density profile of a crystal can be represented in a Fourier expanded form as $\rho_s = \rho_L^{ref}(1 + \eta_s + \sum_K A_K e^{iKr})$,where A_K are the respective Fourier amplitude, η_s is the fractional change in density from liquid to crystal and K is the reciprocal lattice vector. After introducing the reduced number density[11,13] $n = \frac{(\rho - \rho_L^{ref})}{\rho}$ and substituting $\rho = (1 + n)\rho_L^{ref}$, equation(17) of difference in Helmholtz free energy transforms to the following form[10,11]:

$$\frac{\Delta F}{k_B T} = \int dr\left[(\rho_L^{ref}(1+n)\ln(1+n) - \rho_L^{ref} n\right] - \frac{1}{2}\iint dr_1 dr_2 \rho_L^{ref} n(r_1)\rho_L^{ref} n(r2) * C(r_1, r_2) - (18)$$

For further simplification, the product of $\int dr_1 \rho_l^{ref} n(r_1) * C(r_1, r_2)$ is dealt as a Fourier transform of a convolution integral which states that[14]:

$\mathbb{F}(f * g) = \mathbb{F}(f)\mathbb{F}(g), where\ \mathbb{F}\ represents\ the\ Fourier\ Transform\ of\ the\ function\ f$

The convolution integral expression can be written as $\mathbb{F}^{-1}(\mathbb{F}\left(\int dr_1 \rho_l^{ref} n(r_1) * C(r_1, r_2)\right)$ with $\mathbb{F}^{-1}$ being he Inverse Fourier Transform

For reference Fourier transform and Inverse Fourier Transform of any function in Fourier space and real space can be written as per equation 19 and 20 respectively:

$$\hat{f}(\omega) = \int_{-\infty}^{\infty} f(x) * e^{-i\omega x} dx \qquad (19)$$

$$\hat{f}(x) = \int_{-\infty}^{\infty} f(\omega) * e^{i\omega x} d\omega \qquad (20)$$

The integral term in the excess Helmholtz free energy after Fourier transform operation functional breaks down to

$$\frac{1}{2}\int dr_2\, \rho_L^{ref} n(r_2)\mathbb{F}^{-1}(\rho_L^{ref} n(\omega)\hat{c}^2(\omega)) \qquad (21)$$

,where $\hat{n}(\omega)\ and\ \hat{c}^2(\omega)\ represent\ fourier\ transform\ of\ (\rho_L^{ref} \times n(r_1))\ and\ c^2(|r_1 - r_2|)$

Now expanding the Fourier transform of direct correlation function $\hat{c}^2(\omega)$in a Taylor series of terms around ω=0 equation (21) becomes[14]:

$$\frac{1}{2}\int dr\rho_L^{ref} n(r_2)\mathrm{F}^{-1}(\rho_L^{ref} n(\omega)(\hat{C}_0 + \hat{C}_2\omega^2 + \hat{C}_4\omega^4 + \cdots..)) \qquad (22)$$

,where $\hat{C}_2 = \frac{1}{2!}\frac{d^2\hat{C}_0(0)}{d^2\omega}, \hat{C}_4 = \frac{1}{4!}\frac{d^4\hat{C}_0(0)}{d^4\omega}$ and $\hat{C}_K = \hat{C}_0 + \hat{C}_2\omega^2 + \hat{C}_4\omega^4$ has its first peak ω=2π/**σ** ,**σ** being the inter particle distance.

Now we revisit equation (21) and apply the inverse Fourier transform operation to produce an equation in the real space. Here we need to acknowledge an important property of the Fourier transform operation of the nth order derivative of a function and its relation to the Laplacian of the function. The Fourier transform of the derivative of a function $f(x)$ can be evaluated by parts integration in the following way:

$$\int_{-\infty}^{\infty} f'(x) * e^{-i\omega x}dx = [e^{-\omega x}f(x)]_{-\infty}^{\infty} + \int_{-\infty}^{\infty} i\omega e^{-i\omega x}f(x)dx \quad (23)$$

For very large value of x (tending to ∞) f(x) tends to zero. The remaining second term in the above expression can be written as $i\omega\hat{f}(\omega)$ .Similarly it can be proved that the Fourier transform of the second derivative and fourth derivative and so on can be related to the Laplacian of the function as:

$$\mathbb{F}[\nabla^2 f] = -\omega^2\hat{f} \qquad (24)$$

$$\mathbb{F}[\nabla^4 f] = \omega^4\hat{f} \qquad (25)$$

The inverse ($\mathcal{F}^{-1}$) Fourier transform of the functions $\left(\widehat{C_0} + \widehat{C}_2\omega^2 + \widehat{C}_4\omega^4 + \cdots..\right) * \rho_L^{ref} * n\ (\omega)$ in equation (22) and incorporation of relations given in (24,25) results in the following form of the Excess Helmholtz free energy functional [10,11]

$$\frac{\Delta F}{k_B T} = \int dr\left[(\rho_L^{ref}(1+n)\ln(1+n) - \rho_L^{ref} n\right] - \frac{1}{2}\left(\rho_L^{ref}\right)^2 \int dr_1 n(r_1)\left\{\sum_{j=0}^{m}(-1)^m C_{2j}\ \ \nabla^{2j}\right\} n(r_1) - (26)$$

The next step is to introduce the dimensionless form of C_{2j} as $\rho_L^{ref} C_{2j} = \sum_{j=0}^{m} c_{2j}\,\nabla^{2j} = \sum_{j=0}^{m} b_{2j}\,(\sigma\nabla)^{2j}$,where $\boldsymbol{\sigma}$ is the inter particle distance. The coefficients b_{2j} contain information about the physical properties of the crystal and fluid. Expansion of the term ln(1+n) and its product with (1+n) gives

$$(1+n) * \ln(1+n) = n + \frac{n^2}{2} - \frac{n^3}{6} + \frac{n^4}{12}\ for\ |n| < 1 \qquad (27)$$

The equation boils down to the following form[11,13] after logarithmic expansion and b_{2j} inclusion :

$$\frac{\Delta F}{k_B T \rho_L^{ref}} = \int dr\left(\frac{n^2}{2} - \frac{n^3}{6} + \frac{n^4}{12}\right) - \frac{n}{2}\left\{\sum_{j=0}^{m} b_{2j}\,(\sigma\nabla)^{2j}\right\} n \qquad (28)$$

For m=2 PFC model, the equation results in the following manner:

$$\frac{\Delta F}{k_B T \rho_L^{ref}} = \int dr\left\{\frac{n^2}{2}(1+|b_0|) + \frac{n}{2}[|b_2|\sigma^2\nabla^2 + |b_4|\sigma^4\nabla^4]n - \frac{n^3}{6} + \frac{n^4}{12}\right\} \qquad (29)$$

Introducing new variables giving information giving information about the physical attributes of crystal and fluid such as[11]:

$$B_L = |1 + b_0| \ \ [= \left(\frac{1}{k}\right), where\ k\ is\ the\ compressibility] \qquad (30)$$

$$B_s = \frac{|B_s|^2}{4|b_4|}\ [= \frac{K}{(\rho_L^{ref} kT)}\ , where\ K\ is\ the\ bulk\ modulus\ of\ crystal \qquad (31)$$

$R = \sigma(2|b_4|/|b_2|)^{1/2}$ [$= the\ new\ length\ scale$ ($x = R\tilde{x}$, which is now related to the position of the maximum of Taylor expanded $\hat{C}_\omega$] (32)

Including a multiplier $\boldsymbol{\nu}$ for the n^3 term in Helmholtz free energy equation we obtain the following equation:

$$\Delta F = \int drI(n) = k_B T \rho_L^{ref} \int dr \left\{ \frac{n}{2} [B_L + B_S(2R^2\nabla^2 + R^4\nabla^4)]\mathrm{n} - \nu \frac{n^3}{6} + \frac{n^4}{12} \right\}$$

-(33)

Conversion to the phase field Ψ form with additional new variable $x = R\breve{x},\ n = (3B_s)^{1/2}, \Delta\tilde{F} = (3\rho_L^{ref} kTR^d), , \Delta\tilde{F}$ is the free energy into a modified swift -Hohenberg type dimensionless form written as[11,13]:

$$, \Delta\tilde{F} = \int \breve{dr} \left\{ \frac{\Psi}{2} \left[r^* + \left(1 + \breve{\nabla}^2\right)^2 \right] \Psi + t^* \frac{\Psi^3}{3} + \frac{\Psi^4}{4} \right\} - (34)$$

,where $t^* = -\left(\frac{\boldsymbol{\nu}}{\mathbf{2}}\right).\left(\frac{\mathbf{3}}{B_s}\right)^{\frac{\mathbf{1}}{\mathbf{2}}} = -\boldsymbol{\nu}.\left(\frac{|b_4|}{|b_2|^2}\right)^{\frac{1}{2}}\ and\ r^* = \frac{\Delta B}{B_s} = \frac{(|1+b_0|)}{\frac{|b_2|^2}{4|b_4|}}$while $\Psi = \frac{n}{(3B_s)^{1/2}}$.

The equation shows that m=2 PFC model contain two dimensionless similarity parameters $t^* and\ r^*$ that can be obtained as combination of the original physical model parameters. The next section will discuss the derivation of PFC model equation of motion from the underlying concept of time evolution of density as is given by the model of Dynamic Density functional theory.

II-4 Equation of Motion (PFC)

Similar to DDFT based on the concept of conserving relaxation of density profile with time, the equation of motion for a PFC model is derived [11] except that it includes a constant mobility coefficient of $M_\rho = \rho_0 D_\rho / kT$.Thus the equation of motion has the form[11]

$$\frac{d\rho}{dt} = \nabla \left[M_\rho \nabla . \frac{\delta F[\rho]}{\delta \rho} \right] - (39)$$

. When density ρ replaced as reduced number density $n = \frac{(\rho - \rho_L^{ref})}{\rho}$ in equation 39, and incorporating equation 18 transforms to[11,13]:

$$\frac{dn}{d\tilde{t}} = \nabla^2[n\left(|1 + b_0| + \sum_{j=0}^{m}|b_{2j}|\nabla^{2j}\, n - \frac{n^2}{2} + \frac{n^3}{3}\right] \qquad (40)$$

, where. Equation (40) after introducing variable from (31), (32) and (33) becomes

$$\frac{dn}{dt} = \hat{\nabla}\left\{M_n\hat{\nabla}[(kT\rho_L^{ref})([B_L + B_S\left(2R^2\hat{\nabla}^2 + R^4\hat{\nabla}^4\right)]n - \nu\frac{n^2}{2} + \frac{n^3}{3}\right\} \qquad (41)$$

Now following the same sequence of conversion as that for (34) the dimensionless Swift -Hohenberg for PFC Equation of motion follows[11]

$$\frac{d\Psi_\prime}{dt} = \breve{\nabla}^2\left\{\left[r^* + \left(1 + \breve{\nabla}^2\right)^2\right]\Psi + \Psi^3\right\} \qquad (42)$$

, where r* and other operation have been defined previously.

In m=2 PFC model equation of motion is dimensionless with parameter r^* comprising the physical properties of the material. This is the most generic form of PFC model equation of motion used to study of the various aspects of crystallization phenomenon. The next section will discuss some of the previous research work performed via utilizing PFC model to study the essential parameters of a crystallization process.

II-5 Literature review

The model of Dynamical Density Functional theory and Phase Field Crystal model has been applied on numerous occasion to predict a theoretical understanding of the general characteristic of a crystallization process. Through the phase of initial literature review we have broadly classified our review work into three categories which are as follows:

1) Crystal Growth
2) Phase/Facets development
3) Morphology of crystal growth

In the following sections, we have discussed some of the previous work in each of the above categories along with their respective conclusion and results.

II-5-1 Crystal Growth

II-5-1- a- Externally Imposed Nucleation

In this work[15] the fundamental equation of DDFT ($\frac{\partial(\rho(r,t)}{\partial t} = \frac{D}{kt}\nabla.(\rho(r,t)\nabla\frac{\delta F[\rho(r,t)}{\delta\rho(r,t)}$) is solved numerically to study the crystal growth on a nucleation cluster created by an external potential. There are two setups for which the simulation is performed. The first setup has rhombic nucleation seed of 19 particles arranged in a hexagon with different unit cell parameter Area A (strain parameters) and θ spanning the two nucleus axes. The second setup includes the time evolution of a nucleation seed of two equal linear arrays along the *y* direction, each comprising three infinite rows of hexagonally crystalline particles, which are separated by a gap.

In case of the first setup, the evolution of density field of the initially arranged hexagonal cluster of 19 particles is observed to be governed by unit cell parameter i.e. A. This shows that the arrangement of particle which has more unit cell area (less strain) grows into an equilibrium crystalline state while the one with lesser area (more strain collapse into the surrounding metastable liquid).

S**ummary:**

The outcome of this work is relevant to acknowledge Dynamical Density Theory as a powerful tool in investigating heterogenous nucleation on an externally imposed cluster of atoms. It is deduced from these results that initial arrangement of atoms in imposed cluster (area for unit cell) determine whether further crystallization occurs. Moreover, these results coveys a theory that crystallization is a two-step process in which the imposed heterogenous cluster first relaxes with respect to the surrounding fluid and then promotes free growth throughout the space.

II-5-1-b DDFT & PFC for Colloidal Solidification

In this work[16] a comparative study is performed between the phase field crystal theory and DDFT towards analyzing nucleation behavior in a colloidal suspension. The respective equation for DDFT and PFC model that were solved are as given below[16]:

DDFT- $\frac{\partial(\rho(r,t)}{\partial t} = \frac{D}{kt}\nabla.(\rho(r,t)\nabla\frac{\delta F[\rho(r,t)}{\delta\rho(r,t)}$

PFC- $\rho(r,t) = D\nabla^2\rho(r,t) + D.\{\rho(r,t)\nabla\left[Kt^{-1}V(r,t) - \left(\widehat{C_0} + \widehat{C_2}\nabla^2 + \widehat{C_4}\nabla^4\right)\rho(r,t)\right]\}$

To solve these equations the direct correlation coefficients ($\widehat{C_0}, \widehat{C_2}, \widehat{C_4}$) corresponding to the coupling constant potential ($\Gamma = \frac{u_0\rho^{3/2}}{kT}$) are plugged in to the equations. As discussed earlier, these coefficient are the result of evaluating the excess Helmholtz free energy as per RY approximation and Taylor expansion of correlation function c(r,r') in Fourier space(k). The wave vector k bears a relationship with the interparticle distance (**σ**) in real space.

$$\hat{C}_K = \hat{C}_0 + \hat{C}_2\omega^2 + \hat{C}_4\omega^4 - Fourier\ space\ \omega, \widehat{C_0} + \widehat{C_2}\nabla^2 + \widehat{C_4}\nabla^4 - Real\ Space$$

The corresponding value of the direct correlations function $c_0^2(r)$ (determined by correlation coefficients $\widehat{C_0}, \widehat{C_2}, \widehat{C_4}$)against the coupling constant (interaction strength) governs the metstability of the fluid and the stability regime of the crystalline region. Initially the particles were tagged in a liquid with a coupling constant $\Gamma<\Gamma_f$ (freezing) and then quenched to a coupling constant corresponding to a higher correlation among particles to initiate the freezing transition. The snapshot of emergence of density field ρ (r, t) with time for a coupling constant of Γ=60 by solving the DDFT and PFC model numerically has been reported.

Another interesting result which have been tabulated in this work is the y averaged density profile along the x direction. The results demonstrate that variation of ρ(r,t) about the y averaged density (ρ) is more strengthened in case of DDFT than in PFC mode. Also, the

width of the crystal front propagation in case of DDFT ($\Delta x=5\rho^{-1/2}$) is smaller than that of PFC model ($\Delta x=25\rho^{-1/2}$).

The article also reports crystal front propagation velocity $v_f(\Gamma) = \frac{dx_f(t)}{dt}$ as a function of change in coupling constant from $\Delta\Gamma(\Gamma\text{-}\Gamma_f)$ from its initial value to freezing transition value Γ_f. It was well observed, that the crystal front velocities increase with increase in $\Delta\Gamma$. When $\Delta\Gamma$ is negative or the coupling constant $\Gamma<\Gamma_f$, then the crystal front velocity is negative and it retreats to the initial liquid. As calculated from this data the coupling constant for freezing transition in case of the three model is around $\Gamma=36$.

Summary:

The essence of this work comes from the fact that it portrays PFC and DDFT models as powerful tools to study Brownian dynamics of particle in a colloidal dispersion. The derivation of the PFC model was achieved after inculcating certain approximation to the pair correlation function present in the excess Helmholtz free energy functional. Thus, it is reasonable to claim that numerical solutions of DDFT and PFC model equation are effecting in predicting crystal front propagation with time and space.

II-5-2 Phase/Facets Development

II-5-2-a Diffusion controlled growth Polymorphs/phases

This work[17] considers the time evolution of phase field density to study the crystallization of facets of different phases (BCC, FCC, HCP,SC) as a function of one particle number density in a under cooled liquid. The phase field density equation is given by[17]:

$$\frac{dn}{dt} = \nabla.\left(M_n \nabla \frac{\delta F}{\delta n}\right)$$

Where $\Delta F = \int dr \left\{ \frac{n}{2}[B_L + B_S(2\nabla^2 + \nabla^4)]n - \nu \frac{n^3}{6} + \frac{n^4}{12} \right\}$

Here $M_n = \left[\frac{(1+n_0)D_\rho}{k_\beta T \rho_l^{ref}} \right]$ is the constant mobility term determining the time scale for system evolution and n_0 is the initial reduced density of the reference fluid. The dislocation-free growth of the (100), (110) and (111) faces of the BCC and FCC structures, and the (0001) $(10\bar{1}0)$, and $(11\bar{2}0)$ faces of HCP are studied. The facets evolution study is done by the respective reduced density (n_{min}) of the liquid ahead of the growing crystal front. During evolution of crystal front it is observed that there is a certain ordering of liquid at the interface and further crystallization (growth process) is observed by sharp rise in density peaks (n_{max}).

Initially the system is assigned as a rectangular slab of dimension (Δx, Δy, Δz) in increments of $\Delta a=1$. The slab is initially filled with particle density (n) distributed periodically as sin and cosine function of (x,y,z) coordinate of the simulation slab. The driving force of crystallization $\Delta\omega$ (grand potential density) against initial number density n_0 is simulated and reported.

This results analysis reveals that liquid -crystal coexistence for different phases are BCC-Liquid: -0.0862<n0<0.0315, HCP-Liquid: -0.0865<n_0< -0.0344, FCC-Liquid: -0.0862<n_0<-0.0347, SC-Liquid: -0.0.249<n_0<-0.0216. Consequently, numerical solution of PFC Equation of Motion was also carried to study various aspect of crystal growth in a BCC system. The article reports non-uniform density distribution along the centerline in z direction for different BCC crystals facets precipitating from the same far field density representing anisotropic growth. It also reports the density depletion ahead of the crystal front which resembles a barrier controlled layer by layer growth of the BCC crystal. The interface position for different BCC facets with time $\boldsymbol{\tau}$ and the velocity coefficient-C of these facets are some other results produced through this work.

Summary:

The significance of this work is the fact that it was possible to predict the diffusion controlled growth of a BCC, FCC and HCP crystal system coming from a surrounding liquid. The phenomenon of diffusion controlled growth was supported by the fact that density depletion zone between the liquid and crystal varies for different facets of a crystal system (BCC as reported in this article). Moreover, the anisotropic growth in a BCC crystal system was also reported in terms of plots of Interface position vs Time and Velocity coefficient vs Initial Reduced Density(n_0) for respective facets.

II-5-2-b Polymorphism & Crystal nucleation in PFC model in 2D and 3D

This work[11,18] discusses about the thermodynamic driving force (minimization of free energy) which result in the evolution different phases(BCC,FCC,HCP) in a homogenous phase of given density. The equation of motion and Euler Lagrange (free energy minimization with respect to Ψ) were solved numerically to study this phase evolution. These equations are of the following form[11]

Euler Lagrange: $\frac{\delta \tilde{F}}{\delta \Psi} = \frac{\delta \tilde{F}}{\delta \Psi}\Big|_{\Psi_0}$ (Ψ0 minimizes F)

Equation of motion: $\frac{d\Psi\prime}{dt} = \bar{\nabla}^2 \left\{ \left[r^{*\prime} + \left(1 + \bar{\nabla}^2\right)^2 \right] \Psi' + \Psi'^3 \right\} + \alpha^*$

For the respective BCC, FCC, HCP phases the initial guess of the normalized density(Ψ) was assigned as a combination of periodic sin and cosine function in space. On computationally solving the equation of motion (density evolution) it was possible to predict the equilibrium shape of the crystal whose faces are bounded by the planes of BCC, FCC and HCP phases. In a different numerical analysis, the Euler Lagrange equation was solved to predict a 3D phase diagram representing different phase with respect to reduced temperature r* and reduced number density Ψ_0. The three-phase equilibria (liquid–hcp–bcc, liquid–fcc–

hcp, hcp–bcc–rod, and fcc–hcp–rod) are represented by horizontal peritectic/eutectoid lines in the phase diagram.

The other interesting results reported in this article is the 3-dimensional evolution of equilibrium shapes for the FCC, BCC, HCP structures respectively. The equilibrium shapes as predicted comes as rhombo-docodehdral, Octahedral and hexagonal prism structures bounded by (100), (111) and $(10\bar{1}0)$ planes for the respective BCC, FCC and HCP system.

The equilibrium crystal shapes whether BCC or FCC phase is determined after observing the work of formation (grand canonical potential difference) against the number of atoms.

Summary:

This work highlights the effective utilization of PFC model EOM and EL equations to predict polymorphism and various aspect of crystal nucleation. The outcome of the simulation was successful enough to predict a 3D phase diagram representing different phases i.e. Liquid-FCC-HCP-BCC-Rod at different pair values of reduced temperature r*(contains information about the physical properties of the model) and reduced number density Ψ_0 with respect to the reference fluid .The solution of the model reveals the final equilibrium shapes of the nucleated crystals pertaining to BCC,FCC,HCP as rhombo-docodehdral ,Octahedral and hexagonal prism structures bounded by (100),(111) and $(10\bar{1}0)$ planes respectively.

II-5-2-c Heterogeneous Crystal Nucleation: The Effect of Lattice Mismatch

The objective of this work[13,19] was to investigate the process of nucleation on a crystalline substrate. The Helmholtz free energy density expression was modified to include external potential $V_{ext}(r)$ of the substrate. The Helmholtz free energy expression here reads as[19]:

$$\Delta F = \int dr \left\{ \frac{\Psi}{2} [\in + (1 + \nabla^2)^2] \Psi + Vext(r) + \frac{\Psi^4}{4} \right\}$$

, where $\Psi \propto \frac{\rho - \rho_{ref}}{\rho}$ is the scaled density difference, $\in > 0$ is the reduced temperature related to the bulk moduli of the liquid and crystalline phase and is responsible for the anisotropy in crystal growth. The effect of substrate is considered a s an external potential whose properties are managed by the factor **V(r).** This factor which relates to the lattice constant a_s and structure factor $S(a_s,r)$ is added to the PFC Helmholtz free energy expression to introduce the effect of substrate adsorption.

The dimensionless equations which were solved numerically pertaining to this work includes ELE and EOM equation. They read as[19]:

Euler Lagrange Equation $\frac{\delta F}{\delta \Psi} = \left(\frac{\delta F}{\delta \Psi}\right)_{\Psi_0}$ (Ψ_0 minimizes F)

Equation of motion $\frac{\delta \Psi}{\delta \tau} = \nabla^2 \frac{\delta F}{\delta \Psi} + \alpha$, $\alpha\ being\ the\ gaussian\ noise$

The Euler Lagrange equation was solved numerically at reduced temperature of $\in = 0.5\ and\ \in = 0.25$ and varied lattice constant. The solution prescribes the development of non-faceted parallel to a squared lattice wall for parameters $\in = 0.25, \Psi_0 = -0.341$ and $\frac{a_s}{\sigma} = 1.49\ and\ 2$ respectively. However, with parameters $\in = 0.5, \Psi_0 = -0.514$ and $\frac{a_s}{\sigma} = \sqrt{3}\ and\ 1\ respectively$ faceted nuclei growth is observed.

The other phenomenon studied in this work is the growth of a nucleus on a cubic substrate. The dimensions of the cubic substrate Ls are kept at 32 a_s and $16a_s$, where a_s is the lattice constant of a stable BCC structure. Iterative solution showed that with $Ls=32a_s$ the growth on the face of cube is spherical in nature whereas at $Ls=16a_s$ the growth process comes as faceted morphology.

Summary:

In this work the free energy equation of the PFC model was modified to include the effect of external substrate. Thereafter these equations were solved numerically which showed that the lattice mismatch between the substrate and crystal influence the growth morphology of crystal. In addition, these results also convey the idea that the size of the foreign particle effect the final growth morphology of crystal.

II-5-2-d Crystallization induced by multiple seeds: DDFT approach

In this work[20] the process of crystallization was studied by introducing nucleating seeds through an external potential $V_p(r) = \sum_i V_p^0 e^{-\alpha(r-r_i)^2}$ with parameters of the external potential kept as $\alpha\sigma^2 = 6$ and $\frac{V_p^0}{kT} = 4$. To calculate dynamics of crystal growth the DDFT equation was solved numerically which is given by[20]:

$$\frac{d\rho(r,t)}{dt} = \nabla\left[\rho(r,t)\frac{\delta F[\rho(r,t)]}{\rho(r,t)}\right]$$

With this approach, it was observed that the number of particle in each nucleus, the initial orientation and area fraction play a part in grain boundary development between the growing phases. In the first case when the area fraction of the external seeds was kept low the seeds got dissolved and no net growth occurs. In case of an intermediate area fraction and small orientation angle the resultant phase develops as a monocrystal. Finally, in the last case when the orientation angle is large a crystal with grain boundary is formed.

The size ratio of the initial nuclei(N_1/N_2) is another factor which was assumed to play a role in this exact phase behaviour. In the initial setup with N_1=61 and N_2=3, it was observed that the boundary between the monocrystalline phase and the phase with grain shifts towards smaller area fraction. This outcome can be interpreted as lower area fraction being sufficient for the smaller size nucleus to remain stable. In the case when nuclei are kept smaller ($N1$ = 37 and$N2$ = 19), the phase boundary is strongly shifted to higher area fractions. It can be

inferred through this set of simulation results that at low area fractions the bigger nucleus forms a more stable crystal—with larger density peaks and modifies the smaller crystal thus finally filling the entire simulation box and hence no grain boundary or melting is observed.

Summary

In this work, it was successfully demonstrated that DDFT calculation were efficient enough to study crystal growth on an externally imposed multiple nucleation seeds. These results show that there are different scenarios when the initial nucleus grows into a fluid, a monocrystal and crystal with grain boundary. The grain boundary formation and its final position depends upon the size of the nuclei, the area fraction within the fluid and the initial orientation of the seeds with respect to each other.

II-5-3 Morphology

II-5-3-a Tuning the structure of non-equilibrium soft materials by varying the thermodynamic driving force for crystal ordering.

This work[21] discusses the phenomenon of morphological change during crystallization when the thermodynamic driving force are varied in a different set of simulation (Change in particle concentration or level of under cooling of the liquid). The basic PFC equation of motion was solved to study crystal growth on a nucleation seed introduced in a homogenous phase. The Helmholtz free energy is given by[21]:

$$F = \int dr \left\{ \frac{\Psi}{2} [\in + (1 + \nabla^2)^2] \Psi + + \frac{\Psi^4}{4} \right\}$$

The Thermodynamic driving force depends upon:

Supersaturation: $S = \frac{\Psi_0 - \Psi_L^e}{\Psi_S^e - \Psi_L^e}$ and Temperature: $\boldsymbol{\varepsilon}$

The crystal growth was studied for cases when effect of noise was pertinent (thermal fluctuation) along with increase in supersaturation (varying Ψ_0).When the PFC model

equation of motion was solved including the thermal fluctuation the final shape crystal morphology resulted as porous and irregular dendrite, whereas we see a more compact hexagonal morphology when the thermal fluctuation was not included in the simulation.

The other part of this work compares the mechanism of the slow and the fast growth mode (rate of change of supersaturation). The simulation results depict, that a slow growth mode proceeds with evolution of faceted morphology, whereas in a fast growth mode non-faceted morphology develops. Concurrently the simulation results showed that for a slow growth process a sharp and faceted solid–liquid interface builds up at near-equilibrium, whereas in a fast growth process a non-faceted interface builds up which extends to several particle layers. The fast growth process was accompanied by a weak density depletion zone which spread across the solid–liquid interface. The slow growth mode process is further illustrated by simulation results which showed a narrow density depletion zone and a sharp interface

It is claimed through these results that the diffusion mechanism which controls slow mode allows more time to develop a faceted morphology (a sharp interface) unlike the kinetically driven fast mode which results in uniform growth from all facets (interface between crystal and liquid spreads towards many layer).

Conclusion

The results as conveyed and discussed in this work provides a theoretical description to the understanding of crystal growth morphology at different mode. The analysis of these results showed that slow mode of crystal growth is diffusion controlled by thermodynamics whereas the fast mode is kinetically driven.

Chapter III-Results and Discussions

III-1 Experimental deduction

As stated in previous section the fundamental aim of this work is to analyse the morphological phase transition behaviour of charge transfer complex material electro crystallized on a substrate electrode. The experimental results as obtained through the course of this work strongly supports the initial hypothesis of the work. Following the hypothesis, K(def)TCP a charge transfer complex material was electro crystallized on a HOPG substrate under varying condition of initial concentration and applied overpotential. To analyse the role of these parameter on the morphology of electro crystallized K(def)TCP, Atomic force microscopy imaging was performed post the electro crystallization process. The following Atomic force microscopy images given in figure 1 ,2 ,3 depicts the electro crystallization results under respective experimental condition.

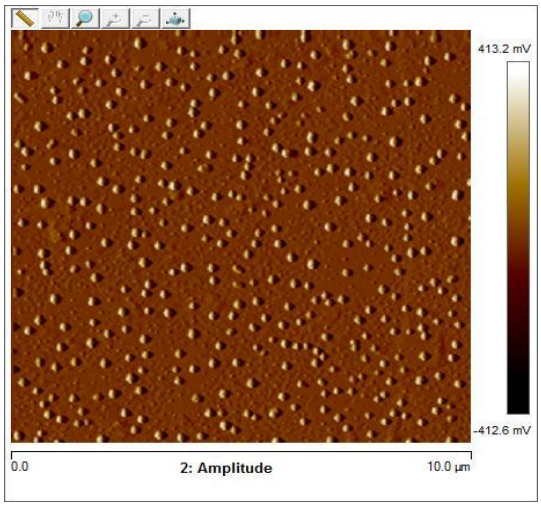

Figure 1- Electrocrystallized K(def)TCP - Concentration: 0.05 M, Overpotential :1.2V and Time of deposition: 1 second

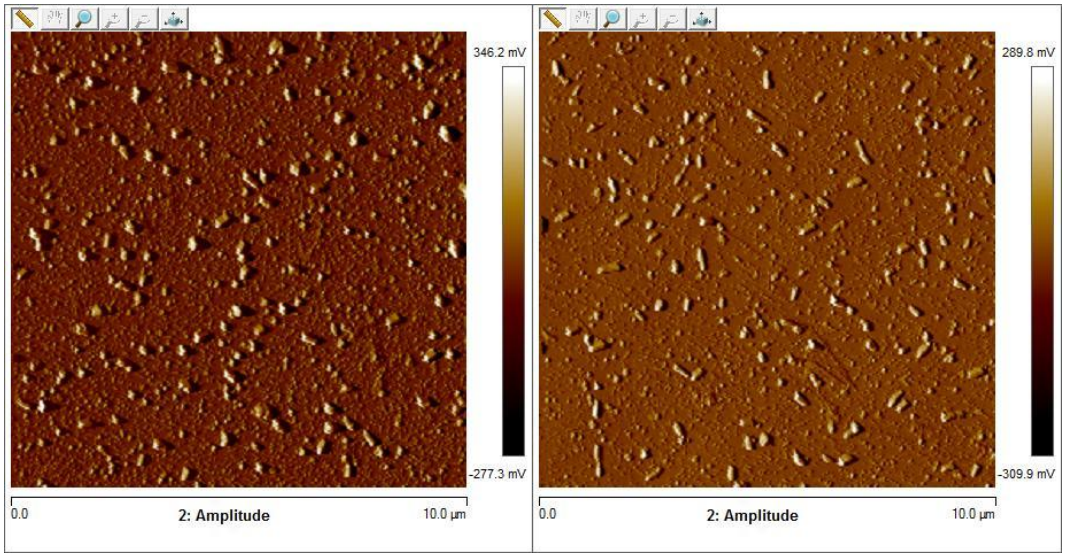

Figure 2- Electrocrystallized K(def)TCP – Concentration:0.2 M, Overpotential:1.2V and Time of deposition:1 second

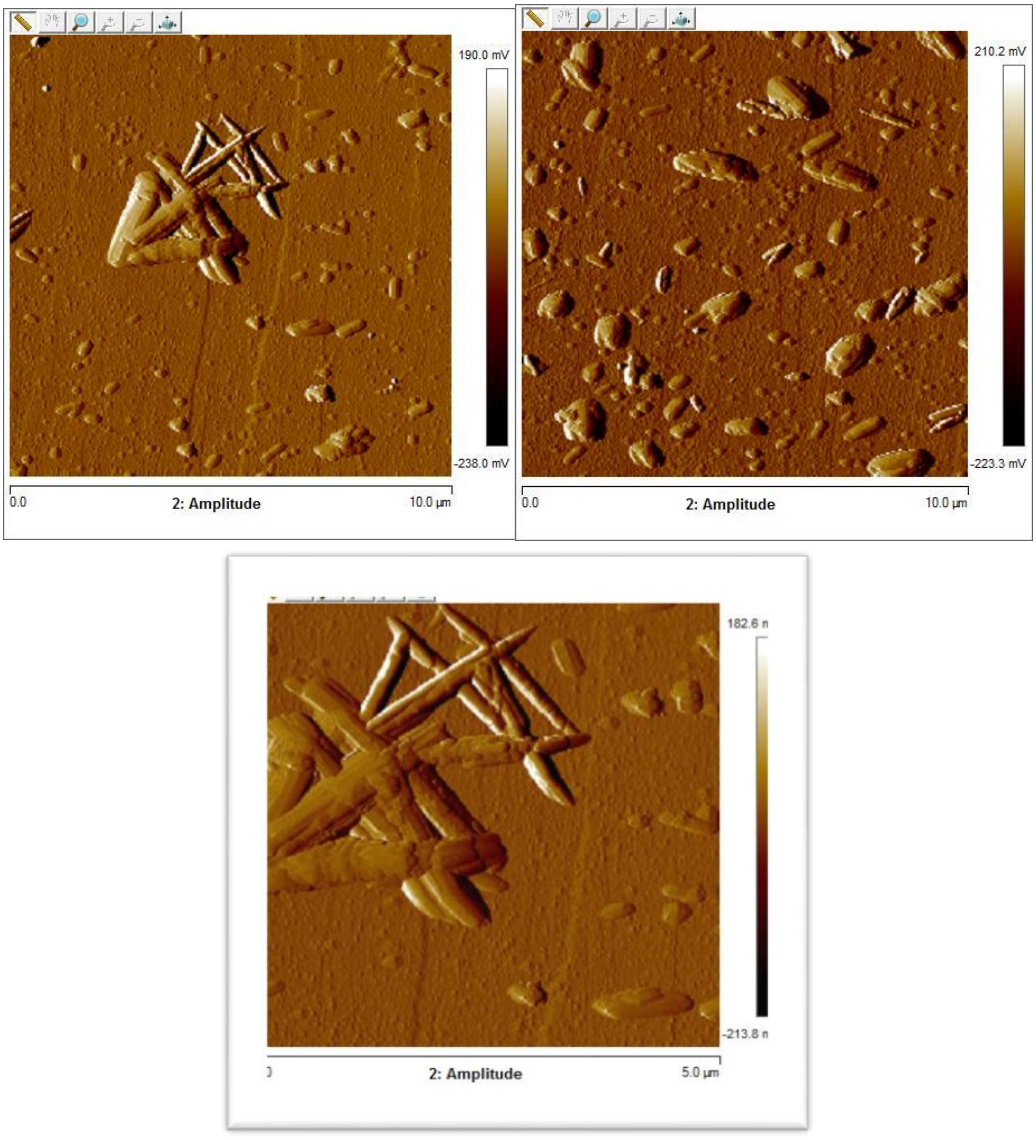

Figure 3- Electrocrystallized K(def)TCP -Concentration:0.2 M, Overpotential: 1.5 V and Time of deposition: 1 second

The experimental results as shown through the above-mentioned AFM images clearly demonstrate that the **morphology** of electro crystallized K*(def)*TCP depends upon the initial experimental parameters takes. The first of the cases (Figure 1) shows that at a low **concentration of 0.05M** and a **overpotential of 1.2 V**, the morphology of the electro crystallized K*(def)*TCP is preferably that of small **spheres** uniformly distributed along the substrate. The morphological transition from spherical to **small rod like** structure (2nd case AFM images) takes place when the K*(def)*TCP concentration was increased to **0.2 M** under the effect of **same overpotential(1.2V)** (Figure 2). Moreover, the rod like morphology of K*(def)*TCP is more prominent when the overpotential is increased to **1.5V** (Figure 3) and K*(def)*TCP concentration is kept at **0.2M**.

The outcome of the experimental work clearly builds up for the argument that morphology of the deposited K*(def)*TCP on the substrate is driven by change in its initial concentration and applied overpotential. Taking into perspective that the electro crystallization process would be governed by the rates of diffusion or deposition of the K*(def)*TCP atoms to the site on the substrate and that the two rates produce a net effect on the morphology of deposited K*(def)*TCP on the substrate. Following on this analysis, it can be argued that the electro crystallization process is thermodynamically driven when rate of deposition lag that of diffusion, whereas kinetic takes over the thermodynamic of the process in the reverse case scenario. Thus, the motivation arises implement Phase Field Crystal model for our theoretical study whose inception comes from the basic concept classical thermodynamics.

III-2 - Theoretical results

The Phase Field Crystal model is derived after making necessary approximation to the Classical Density Functional model. The Helmholtz free energy functional in the PFC model as derived and discussed in the previous chapter takes the following form[11]:

$$\Delta\tilde{F} = \int \widetilde{dr}\left\{\frac{\Psi}{2}\left[r^* + \left(1 + \breve{\nabla}^2\right)^2\right]\Psi + t^*\frac{\Psi^3}{3} + \frac{\Psi^4}{4}\right\} \quad (1)$$

The equation is dimensionless in Ψ which is the relative phase variable given by the ratio of density difference between the one particle density of the crystal and a reference liquid to the one particle density $\frac{(\rho-\rho_L^{ref})}{\rho}$. The variable r^* is the model parameter incorporates the effect of correlation coefficient ($\hat{C}_0, \hat{C}_2$) introduced after expanding the correlation function $\hat{C}_K = \hat{C}_0 + \hat{C}_2 k^2 + \hat{C}_4 k^4$ in fourier space(k). At this point it's a tangible fact that variable r^* and the initial Ψ (reduced particle density) are two major properties which effect the phase equilibrium between the periodic phase(Solid) and a homogenous phase(liquid) with time. Having done a comprehensive review of the basics of the PFC model, it seemed relevant for us to go ahead and investigate the direct correlation function $C(r, r')$ from the view point of classical thermodynamics.

III-2-a- Direct correlation function

To determine the direct correlation function for a system through a model present in literature we referred to the **Ornstein-Zernike Percus-Yevick** (OZPY) equation[22]. The OZPY is one of the most basic equation and is considered a good fit to generate the pair correlation function of simple fluids interacting via Lennard Jones potential. It is of the following form[22]:

$$g(r, r') - 1 = C(r, r') + n * \int C(r, r') * [g(r'', r') - 1]dr'' \quad -(2)$$

, where n is the homogenous density distribution and thus is kept constant. The term kT is the thermal energy in terms of Boltzmann constant (k) and Temperature(T).

The Pair Correlation function $g(r,r')$ in OZPY integral equation bears a linear relationship with the direct correlation function $C(r,r')$ along with an integral including the interaction of a particle placed at $r''(g(r'',r'))$.The equation also incorporates the Percus-Yevick approximation which correlates the pair correlation with the direct correlation function is as follows[22]:

$$C(r,r') = g(r,r')\left[1 - exp^{\frac{u(r,r')}{kT}}\right] \qquad (3)$$

, where $u(r,r')$ is the potential (Lennard Jones ($r^{-6} - r^{-12}$)) acting between the particles. We have performed our simulation run by choosing the units of $u(r,r')$ in unit of thermal energy (kT).

The OZPY equation is not in its simplest form because of the occurrence of $g(r,r')$ and $g(r',r'')$ which makes the solution of pair correlation function in Cartesian coordinates unreasonable. Thus, follows the need to simplify the integral part of the OZPY equation in polar coordinates (r'',θ,φ) which results in the following form of equation:

$$Integral = \frac{2\pi}{r'}\int dr'' g(r,r'') \int_{|r''-r'|}^{r''+r'} r_{12} dr_{12}[g(r12) - 1] \qquad (4)$$

Including the integral, the OZPY equation which we have numerically solved for the direct correlation function

$$y(r,r') = 1 + n * \frac{2\pi}{r'}\int dr'' g(r,r'') \int_{|r''-r'|}^{r''+r'} r_{12} dr_{12}[g(r12) - 1] \qquad (5)$$

, where $y(r,r') = g(r,r') * exp^{\frac{u(r,r')}{kT}}$

Figure 4 is the plot of the pair correlation function g (r, r') at a reduced temperature of 2($u(r,r')$ in units of thermal energy (kT)). The graph gives the plot of the pair correlation function for two different values of homogenous density n in the OZPY equation. The effect of high homogenous density n is evident from the red curve compared to that of low homogenous density given by green curve. The simulation results presented here are at a reduced temperature of ($\beta = \frac{1}{kT}$) 2 and homogenous density of 0.55 and 0.25.

The pair correlation plot in figure 4 is evidence of the fact that the initial homogenous density of the liquid influences the pair correlation and the arrangement of atoms around a reference atom. The red curve represents the case of a higher density homogenous phase (0.55) and have two peaks showing higher packing of atoms. On the other case the green curve with a lower initial density distribution has only one prominent peak implying lesser correlation/packing among atoms.

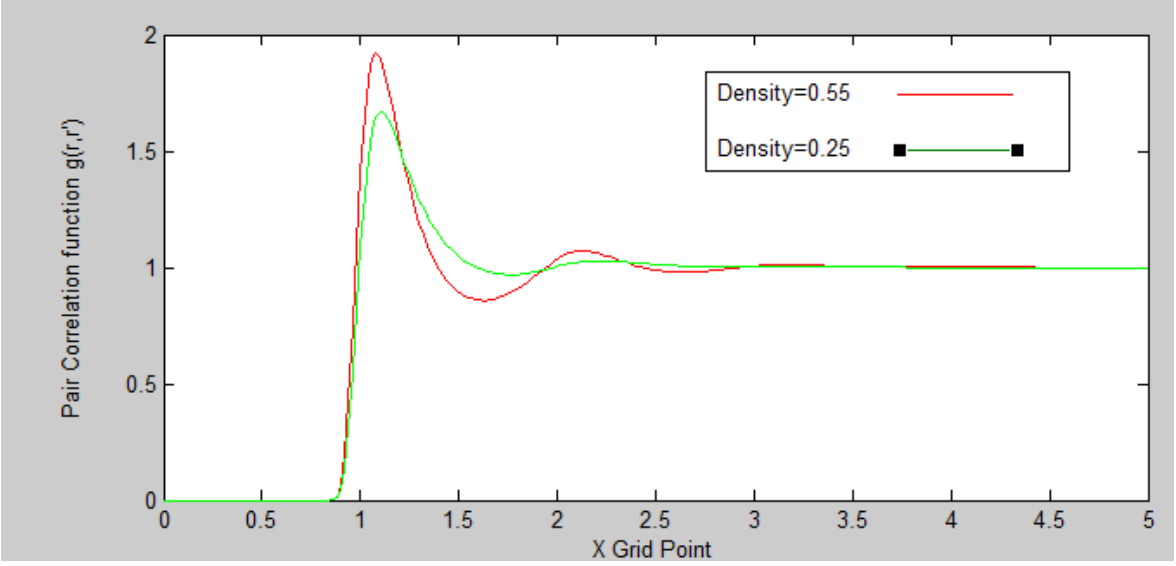

Figure 4- Pair Correlation function for Homogenous density 0.55 (red curve) and 0.25 (green curve).

From here onwards, we refer back to the percus-Yevick relation (equation 2) to compute the direct correlation function ($C(r,r'$) from the pair correlation function ($g(r,r'$).At this point

we may go forward and expand the direct correlation in Fourier space as $\hat{C}_K = \hat{C}_0 + \hat{C}_2 k^2 + \hat{C}_4 k^4$ and calculate r* parameter of the PFC model from these coefficient. This facilitates the use of the PFC model to study the phase behaviour (Ψ) for a fluid or an ideal gas interacting via Lennard Jones potential. However due to the unknown nature of the interacting potential between atoms/ions in solid and periodic phases the solution of direct correlation function though this method becomes trivial and unthinkable. Considering this problem, it is usually recommended to use a numerical value of r*(sometime referred to as reduced temperature) as an initial guess which is close enough to the physical properties (compressibility, Bulk modulus) of the material/phase to be studied through the model. In the next section, we will discuss some of the results we have produced on solving the equation of motion of the PFC model in 1 dimension.

III-2-b Equation of motion

In the previous section, we have discussed the Helmholtz free energy functional (equation 1) of the PFC model. However, the free energy equation that we have simulated in this work is modified to the simplest form possible. For instance we have solved the equation of motion without considering the multiplier t^*as it accounts for the complex contribution of three particle correlation [11] .Moreover we have solved the PFC equation of motion on the standard length scale(x) rather than the scale $\hat{x} = \frac{2*\left(\frac{C_4}{C_2}\right)^{\frac{1}{2}}}{x}$ (corresponds to the maximum of correlation function) on which the Helmholtz free energy of the conventional PFC model has been derived .Incorporating these modification the expression for the Helmholtz free energy we arrive to is given by:

$$\Delta F = \int dr \left\{ \frac{\Psi}{2} [r^* + (1 + \nabla^2)^2] \Psi + \frac{\Psi^4}{4} \right\}$$

The corresponding equation of motion to this form of Helmholtz free energy thus takes the following form:

$$\frac{d\Psi}{dt} = \nabla^2\{[r^* + (1+\nabla^2)^2]\Psi + \Psi^3\} \qquad (6)$$

Equation 6 is a sixth order differential equation which needs a set iterative method to solve over time. To solve the equation in one dimension we have implemented forward Euler Scheme (finite difference) where each iterative step is as follows

$$\Psi_{t+\Delta t,n} = \Psi_{t,n} + \Delta t * \nabla^2\{[r^* + (1+\nabla^2)^2]\Psi + \Psi^3\}$$

The Laplacian and higher order differential in the equation are solve based on finite difference scheme and Discrete Fourier Transform algorithm. As Per the finite difference scheme the Laplacian of the phase variable Ψ at any x position in space and time t is given by

$$\frac{\partial^2 \Psi}{\partial x^2} = \frac{\Psi_{t,x-\Delta x} + \ 2 * \Psi_{t,x} \ + \ \Psi_{t,x+\Delta x}}{(\Delta x)^2}$$

We have solved the equation of motion by plugging in an initial distribution of Ψ along space and value of r* in equation of motion.

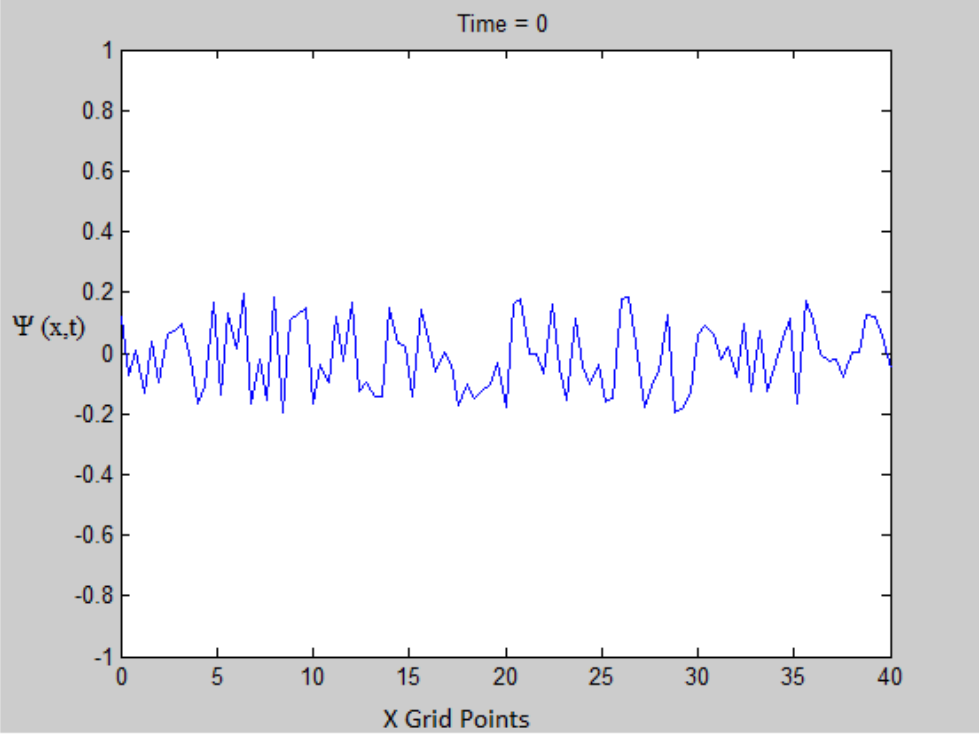

Figure 5- Random distribution of Ψ at Time =0

Figure 5 represents the distribution in space where phase variable Ψ is initialized as random fluctuation around zero resembling initial perturbation in a homogenous liquid. The space variable is discretized as Δx=0.4. The value of r*(reduced temperature) chosen is 0.4 for this case and the simulation is run for 20 units of time at an increment of 0.0001. Figure 6 gives the distribution of Ψ at Time=20.The boundary condition are taken periodic in nature. As is can be observed from Figure 6 Ψ has changed from a random fluctuation to a more periodic phase. This behaviour can be inferred as an effect of sudden undercooling of the liquid by the factor r*=-0.4 in space which results from a random fluctuation into a periodic ordered phase. Our simulation results and the reasoning that follows it seems coherent with the physical mechanism behind the liquid-solid transition in a solidification process.

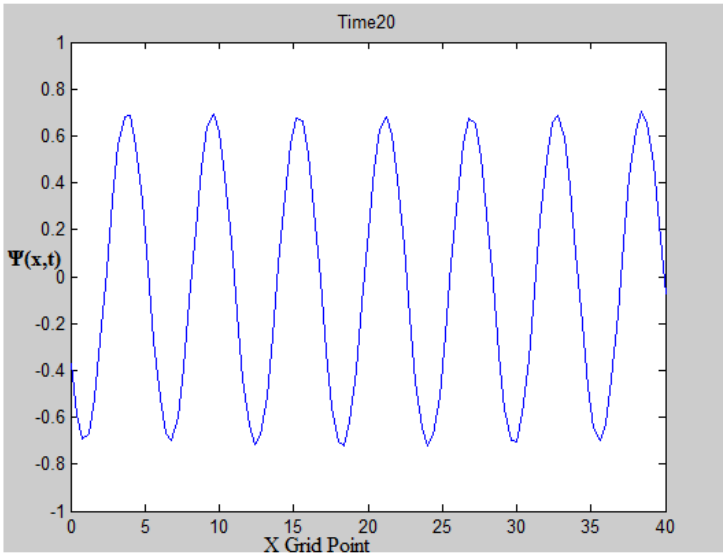

Figure 6- Periodic phase distribution of Ψ at Time =20

We next fitted the periodic phase distribution of figure 6 to a Sin function of the form $Asin(kx - x_0)$,with k as the wavenumber. On number of trial we found that $0.6 * \sin(1.1x)$ best fit the periodic phase distribution at r*=-0.4;

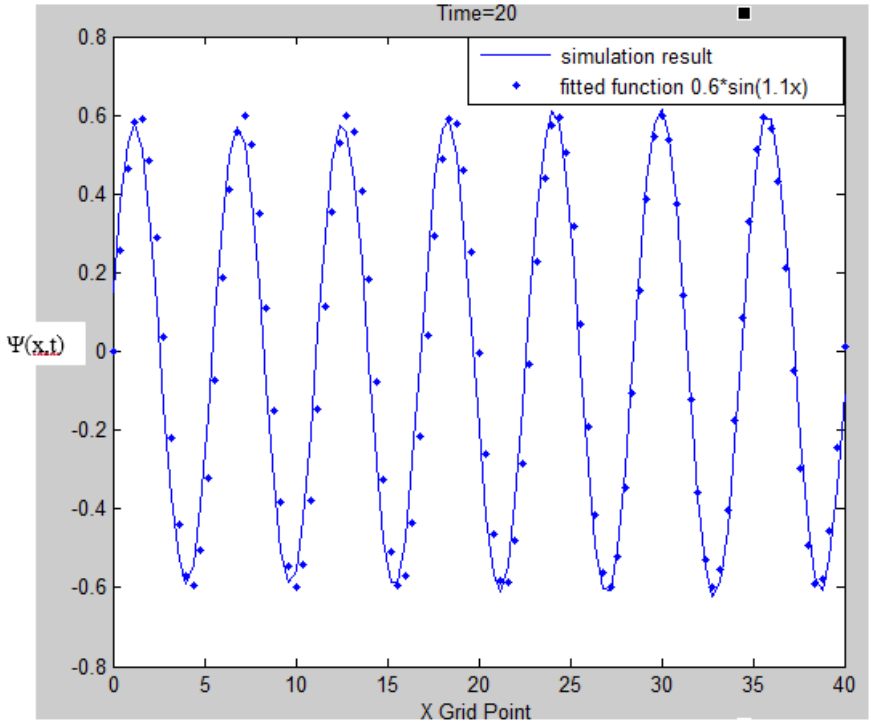

Figure 7- Ψ obtained from initial random fluctuation fitted with a periodic function at r*=-0.4

The results observed in Figure 6 after iteratively solving the PFC equation of motion with initial parameters shows the utility of the model to study transition between two phases (random to periodic) with time. As discussed above we fitted this periodic phase to a Sin function of the form $Asin(kx - x_0)$ and could obtain reasonable results. For our next case, we believed that it was necessary to study the effect of change of model parameters on the phase transition behaviour. On that note we ran few other simulations by placing a crystal in a homogenous phase of reduced density Ψ_0.For that purpose Ψ was initialized as a periodic phase of the form ($A * \sin(kx) + \Psi_0$) for certain portion in space. We initialized the wave number k as 1. The simulation run was performed for different pair of r* and Ψ_0.Figure 8 and 9 gives the simulation results at time t=0 and t=10 for the case with Ψ taken initially as $0.72 * sin(x) + 0.45$.

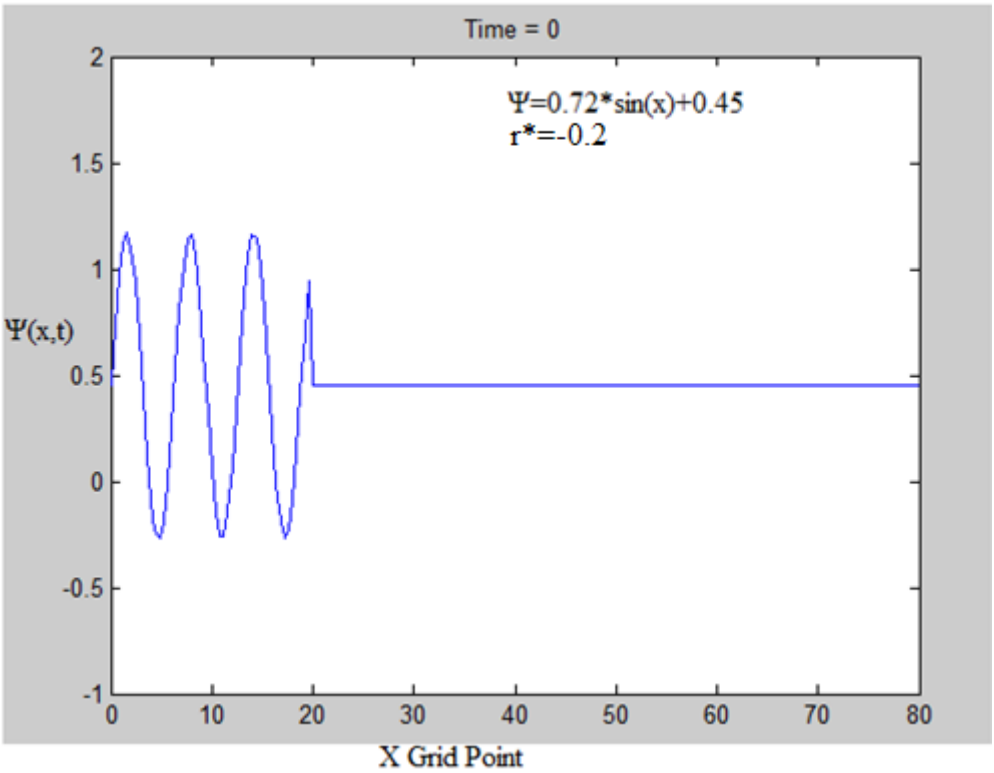

Figure 8- Placing a crystal with periodicity Ψ=0.72*sin(x)+0.45 in a homogenous phase at time t=0 and driving force for solidification given by r*=-0.2

Figure 8 and 9 shows the phase transition Ψ from t=0 to t=10 at the initial quench given by r*= -0.2. The crystal with periodicity Ψ=0.72*sin(x)+0.45 placed in the homogenous phase disappears and cease to grow at this value of quench(r*=-0.2) parameter and reduced particle density $\Psi_0 = 0.45$.

We next considered a different pair of value for Ψ_0 and r*.Figure 10 and 11 gives the simulation results at time t=0 and t=10 respectively. The value assigned to Ψ_0 and r* in this case are 0.2 and -0.45. Figure 10 resembles a crystal with perodicity **Ψ=0.72*sin(x)+0.2** placed in a homogenous phase with reduced density (Ψ_0) **0.2**. As is evident from the result given in Figure 11 the crystal has fully grown across the interface crystal/liquid by time t=10. The simulation results as shown in Figure 9 and 11 are of extreme relevance to determine equilibrium existence or coexistence of crystal/liquid phase along the independent variation of quench parameter(r*) and reduced particle density (Ψ_0).These results holds good to

predict the liquid-crystal phase transition from inherent material properties given by r* and the homogenous phase(with reduced density Ψ_0) surrounding it.

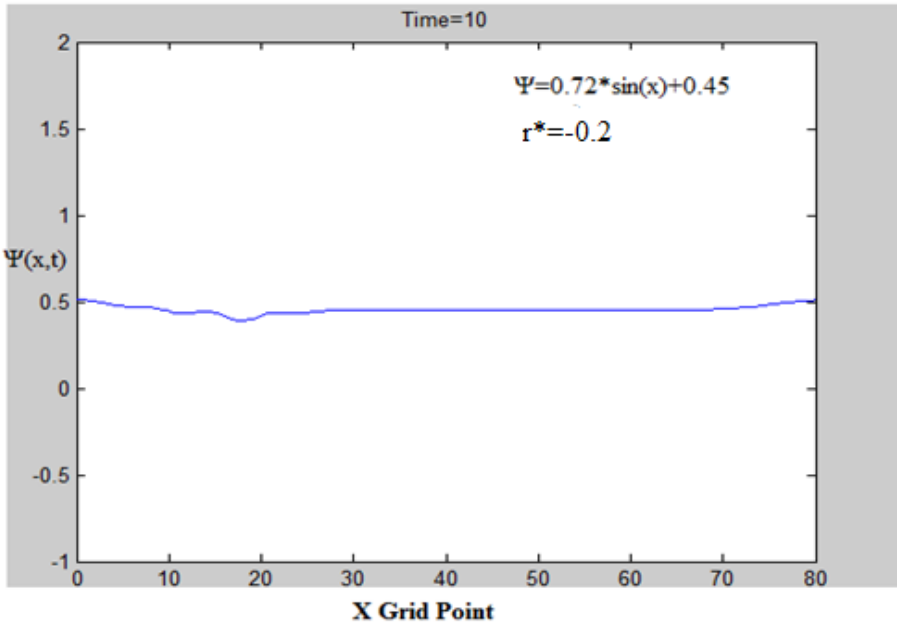

Figure 9- Crystal placed in liquid disappears at time t=10 when the parameter r*=-0.2

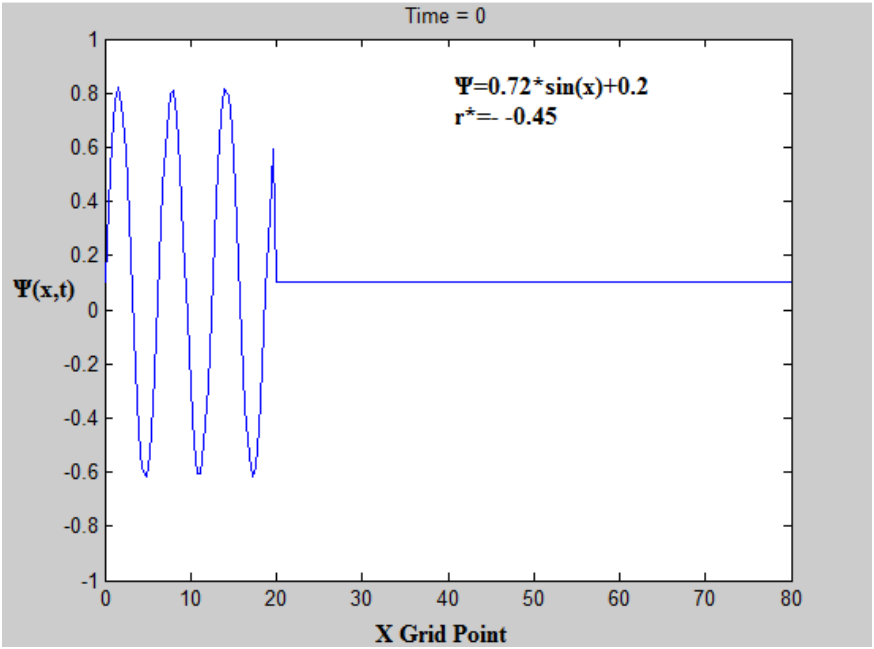

Figure 10- Placing a crystal with periodicity Ψ=0.72*sin(x)+0.2 in a homogenous phase at time t=0 and driving force for solidification given by r*=-0.45

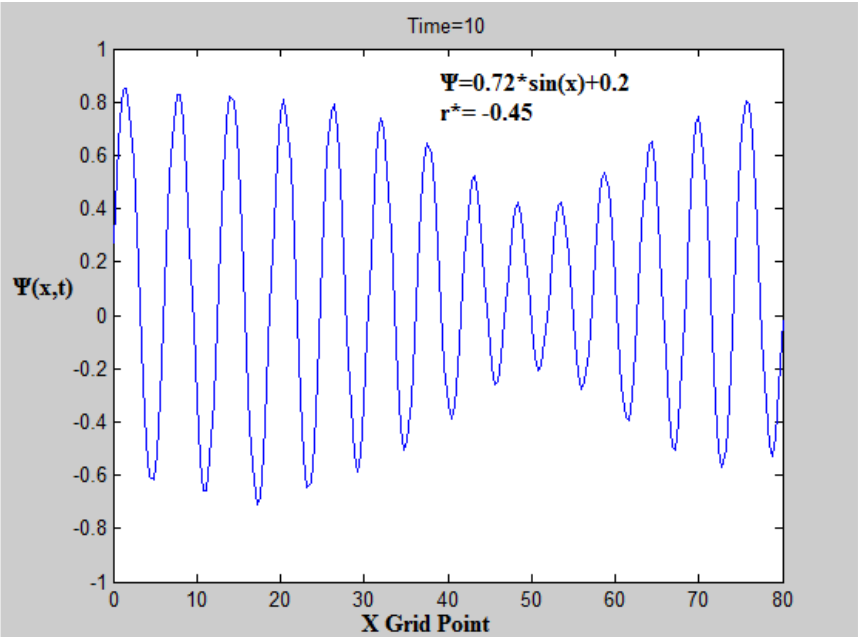

Figure 11- The initial crystal with periodicity Ψ=0.72*sin(x)+0.2 disappear in the homogenous phase after time t=10 when the driving force for solidification is r*=-0.45

We next attempted to look into the interface that gets generated when the Crystal/liquid phases tends to coexist.In order to investigate the interface we first placed the crystal(Figure 12,Time=0) coexixting with a liquid phase and let the system move towrads equlibirum according to the dynamics of PFC equation of motion.We reported our results at time=40 (Figure 13) with quench paramter set at r*=-0.3 and different value of reduced density, $\Psi_{0,l} = -0.43 \; and \; \Psi_{0,c} = -0.29$ .Here $\Psi_{0,l}$ and $\Psi_{0,c}$ represents the boundary between liquid/coexistance and solid/coexistance phase.The hyperbolic tangent fucntion were fitted to the interface between the crystal and liquid on both side as shown in Figure 13. In a similar way we solved for the solid/liquid interface with r*=-0.5 as given in Figure 14.The Crystal /liquid interface in Figure 13 is less steep/sharper compared to that of Figure 14.It is evident from these results that a increase in quench factor r* changes the diffusive width of the interface between crystal and liquid.This shows that at higher quench rate kinetic effects takes over and does not provide sufficient allowance for diffusion effects as per thermodynamic laws.

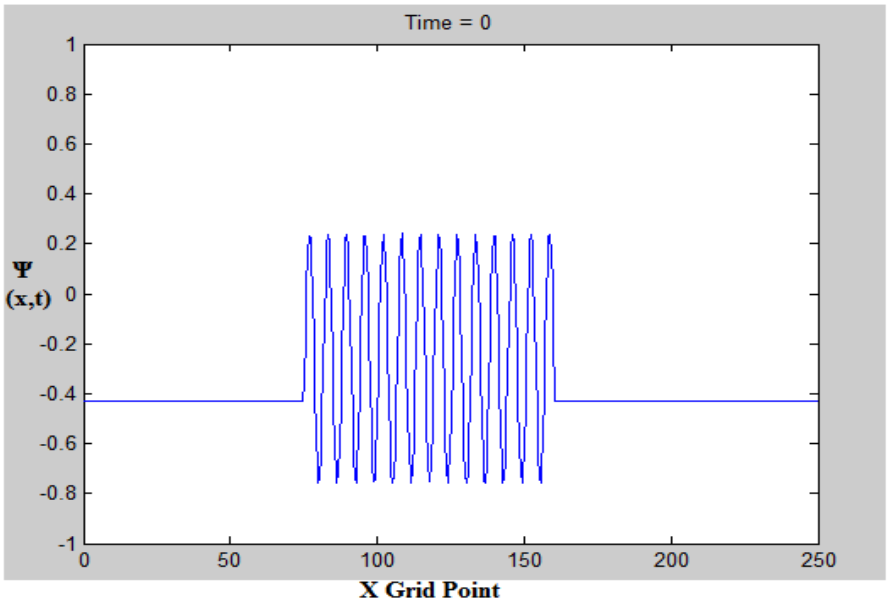

Figure 12- Crystal placed in a liquid at time =0.

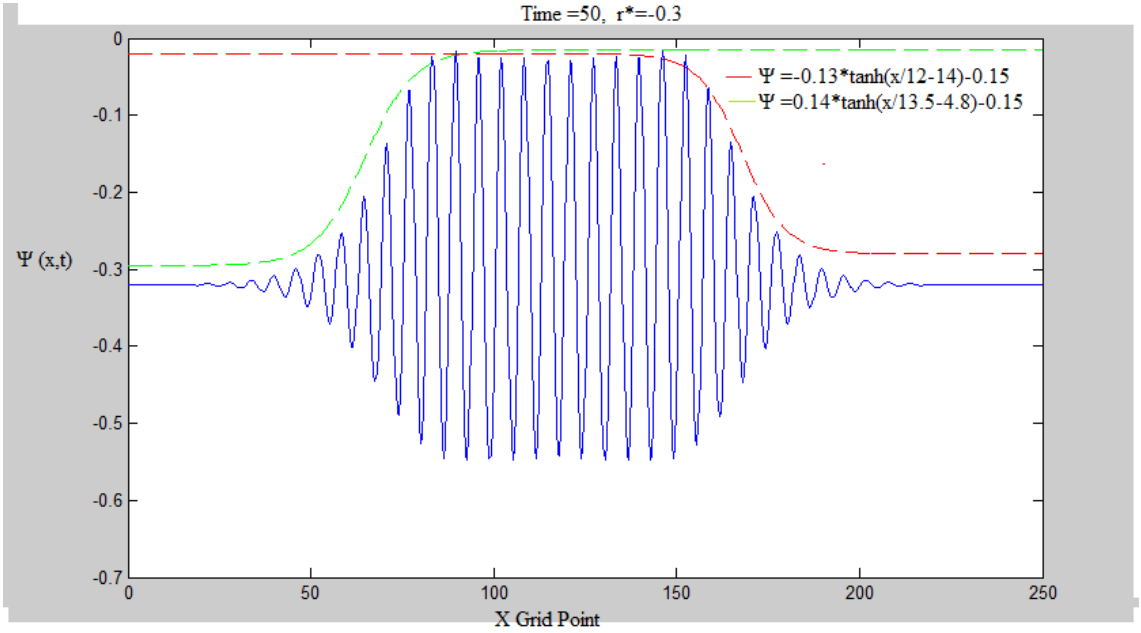

Figure 13- Interface between Crystal/Liquid with parameters r*=-0.3

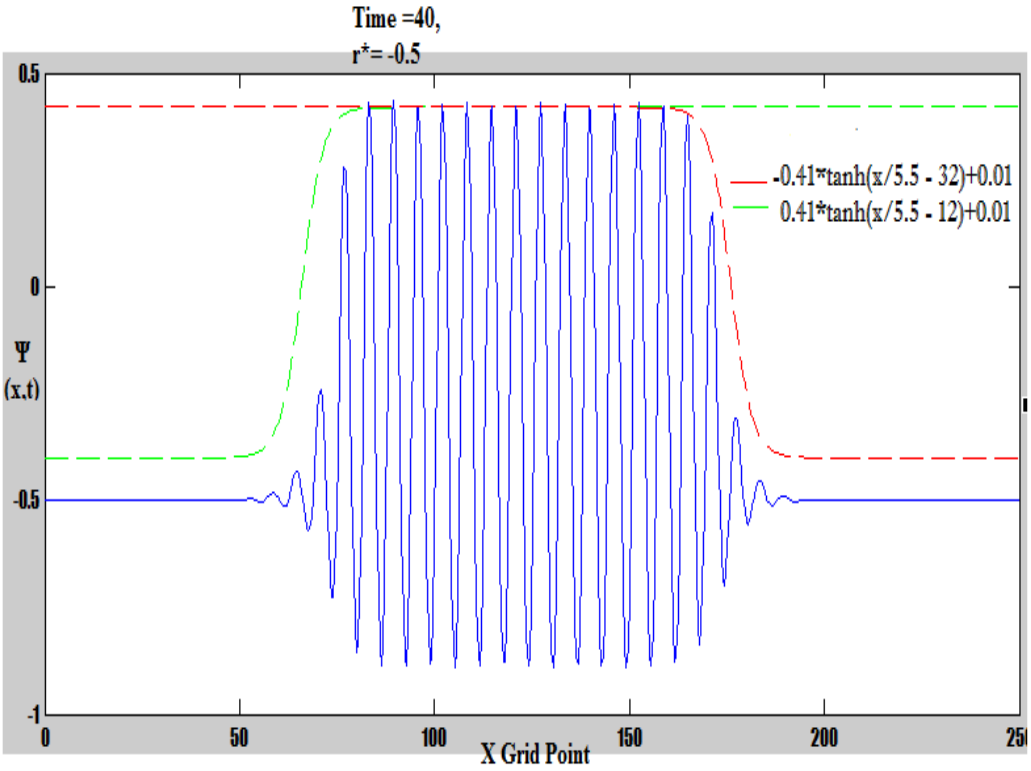

Figure 14- Interface between Crystal/Liquid with parameters r*=-0.5. Interface formed here is sharper compared to the case of r*=-0.3(Figure 31)

III-2-c The Spectral Method

In this section we present some of our simulation results produced using the Fast fourier transform spectral method.The specral method is perceived to be computationally efficient than the finite difference because its uses a simpler method to calculate the higher order derivative.The algorithm of Fast Fourier Transform works by transforming a space dependent function as in our case to frequency dependent (ω) function.We have used the discrete fourier transform of the function Ψ(j) where j range from 1 to N given by:

$$\Psi(\omega) = \frac{2*\pi}{N}\sum_{j=1}^{N} exp^{-i\omega x(j)}\Psi(j) \quad ,$$

Where: ω=[-N/2+1,……..,N/2] and the inverse Fourier transform is given as:

$$\Psi(j) = \frac{1}{2\pi}\sum_{\omega=-\frac{N}{2}+1}^{\frac{N}{2}} exp^{i\omega x(j)}\Psi(\omega)$$

If Ψ(j) is Fourier transformed as $\widehat{\Psi}(\omega)$ then the Fourier transform of higher order derivative of Ψ(j) bears the following relation with

$$\mathcal{F}[\nabla^2\Psi(j)] = -\omega^2\widehat{\Psi}(\omega)$$

$$\mathcal{F}[\nabla^2\Psi(j)] = \omega^4\widehat{\Psi}(\omega)$$

Incorporating these relations makes Helmholtz free energy functional of the PFC model looks like

$$\frac{d\Psi}{dt} = -\omega^2(r * +(1-\omega^2)^2)\widehat{\Psi} - \omega^2\widehat{\Psi^3} \qquad (7)$$

The above equation contains a linear and nonlinear term($\widehat{\Psi^3}$) .Thus we need to operator split the above equation i.e we solve the linear and non linear part separately and then merge the invidual results afterwards. Therefore we solve the linear and non linear part of differential equation separately and apply the forward Euler scheme which results in a numerical solution of the form

$$\widehat{\Psi}(t+\Delta t) = \widehat{\Psi}(t)exp^{L_\omega \Delta t} - \Delta t k^2\widehat{\Psi^3} \qquad (8)$$

Where $L_\omega = -\omega^2(r * +(1-\omega^2)^2)$

The vector ω in this instance is the fourier space frequency variable given by

$$\omega = [0, \Delta\omega, 2\Delta\omega, \ldots\ldots\frac{\pi}{\Delta x}, -\frac{\pi}{\Delta x} + \Delta\omega, -\frac{\pi}{\Delta x} + 2\Delta\omega, \ldots\text{-}\Delta\omega]$$

Here $\Delta\omega = \frac{2\pi}{N\Delta x}$, N being the size of the vector in x space.

We ran our simulation on equation (8) iteratively over time .In each of the simulation we descritized space variable Δx=0.1 and time Δt=0.0001.The system size in real space range from x=-400 to 400. The utility of fourier transform alogorithm in simplifying the higher order

derivative gives us an edge to solve the PFC equation of motion for a larger size system and higher computational speed.Figure 15 gives the simulation results of equation 8 with quench factor r*=-0.7 at time =35.For comparative analysis of this result we performed similar simulation on equaiton 8 with quench factor r*=-0.2 at time =35.

The solution of the PFC equation of motion given in Figure 15 and 16 shows that the quench paramter r* determines the crystal propogation.A higher value of r* accounts for the crystal front propagating to larger length than a lower r*.This deduction falls in line with our earlier analysis made through finite difference alogorithm.

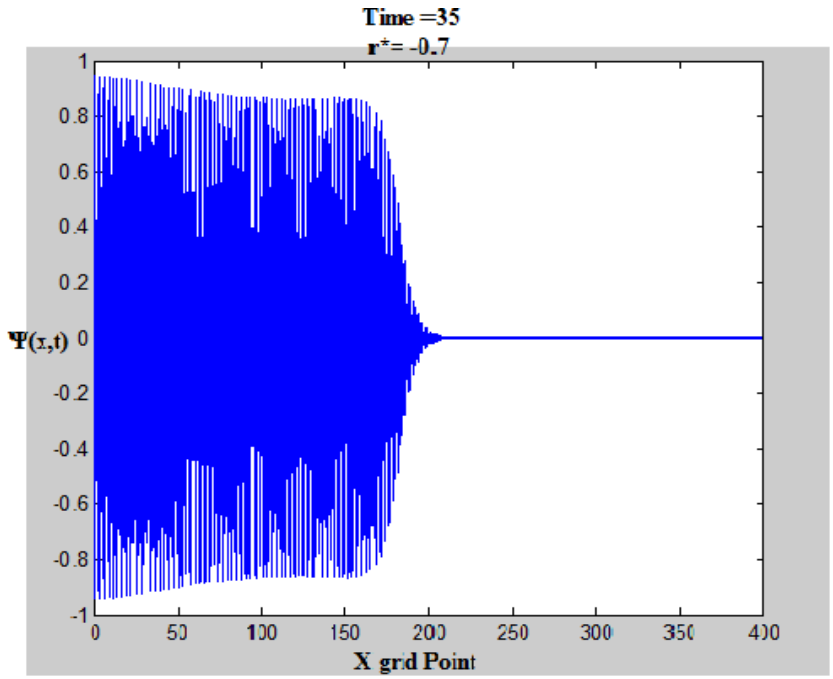

Figure 15- Propagating crystal front at r*=-0.7. The figure only shows the right side of the crystal

.

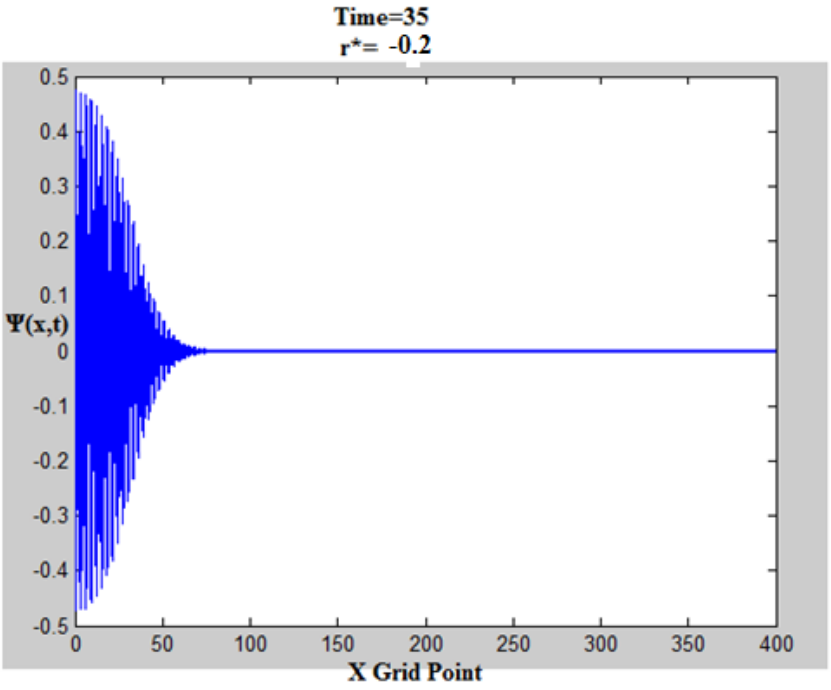

Figure 16- Propagating crystal front at r*=-0.2. The figure only shows the right side of the crystal

Chapter IV-Conclusion

In this work, we have tried putting up a sincere effort to analyse the phase transition behaviour during a crystallization process. The analysis of the experimental results on electro crystallized charge transfer complex material on a substrate electrode laid the initial foundation of our research. The morphological transition of these charge transfer complex materials under different condition of concentration and applied overpotential were relevant results to adopt phase field crystal model(PFC) for our theoretical work. The phase field crystal(PFC) is an effective model to study the equilibrium between a homogenous(liquid) and a periodic phase(crystal). The equilibrium state of the system in a PFC model is represented in terms of Helmholtz free energy functional of density profile. The relation between the change in density profile with time and the proportional change in the Helmholtz free energy with respect to this density profile is referred to as the PFC equation of motion. We have solved the PFC equation of motion for different parameters and have achieved decent quantitative results. We have argued through our results that growth or disappearance of a periodic phase in a homogenous phase depends upon the initial parameters r* and Ψ_0. We have also determined the nature of interface region between coexisting phases through our simulations. We have performed these simulations using the finite difference and Fast Fourier transform algorithm. We have realized through our analysis that the implementation of Fast Fourier Transform significantly increases the computational speed and allows simulation of large system than with the finite difference scheme. These results are encouraging to claim that the PFC model is a powerful tool to correlate with the real time behaviour during a crystallization process.

Chapter V-Future work

The results and data reported in this thesis holds significance for further study of the phase transition phenomenon during the process of crystallization. We have structured our research based on the preliminary demonstration of phase transition behaviour of charge transfer complex material subjected to electro crystallized on a substrate electrode. These results laid initial ground work to adopt the well-known Phase field crystal(PFC) model for our theoretical study. The simulation results of this work are concrete evidence of the point that PFC model is a powerful tool to investigate research problems related to the crystallization process. We have used the most fundamental PFC model for our work in which the driving force for transition between a periodic and homogenous phase depends solely on quench parameter r* and reduced particle density. However, the interaction of charged species in an electro crystallization process it requires necessary modification of the PFC model currently implemented in this work. Moreover, we have restricted the PFC model simulation to 1 dimensional system and have left sufficient space to implement the model to higher dimensions. Our simulation results are encouraging and are a step in the direction to consider PFC for enhanced theoretical study of crystallization process. In a future study, the excess Helmholtz free energy functional of classical density functional theory containing the direct correlation function will change to incorporate the electrostatic interaction among particles. It is worth mentioning that there have been successful attempts to use a modified form of the original CDFT[23] in systems with charged hard sphere[24,25], asymmetric electrolyte[26] .Therefore, a new form of PFC model derived from these modified CDFT model will certainly alleviate the understanding of electro crystallization process on a larger scale..

APPENDIX

Matlab code solving PFC using **Finite difference**

```
clc
clear all
dr=0.4;
x=0:dr:40;
dr2=dr^2;
m=zeros(1,length(x));
Si=-0.2+0.4*rand(1,length(x));      % Si taken as initial random
distribution

f1=figure;
plot(x,Si); % Plotting Si at time=0
  axis([0 40 -1.5 1.5])
 title('Time = 0');
 f2=figure;
 t=50;
dt=0.0001;
epsilon=0.2;

for i=0:dt:t
Si3=Si.^3; % Si^3 calculated from Si
    Si_old=Si;     % Current Si
        for j=1:length(Si)
     cnt=j+1;
      cnt1=j-1;

      if (cnt==length(Si)+1)
          cnt=1;     % applying periodic boundary condition to Si
      end
      if (cnt1==0)
          cnt1=length(Si);  % applying periodic boundary condition to
Si
      end
     term1(j)=(Si(cnt)-2*Si(j)+Si(cnt1))/(dr2);  % Taking Laplcian of
Si at each grip point
          term4(j)=(Si3(cnt)-2*Si3(j)+Si3(cnt1))/(dr2);     % Taking
Laplacian of Si^3 at each grid point
        end
    for k=1:length(term1)
        cnt2=k+1;
        cnt3=k-1;
      if (cnt2==length(term1)+1)
          cnt2=1;       % applying periodic boundary condition to
laplacian of Si
      end
      if (cnt3==0)
          cnt3=length(term1); % applying periodic boundary condition
to laplacian of Si
      end
      term3(k)=(term1(cnt2)-2*term1(k)+term1(cnt3))/(dr2);%   Taking
Laplacian^2 of Si at each grid point
    end
    for l=1:length(term3)
        cnt4=l+1;
        cnt5=l-1;
```

```
            if (cnt4==length(term3)+1)
               cnt4=1;              % applying periodic boundary condition
to laplacian^2 of Si
            end
            if (cnt5==0)
                cnt5=length(term3); % applying periodic boundary condition
to laplacian^2 Si
      end
            term2(l)=(term3(cnt4)-2*term3(l)+term3(cnt5))/(dr2);   % Taking
Laplacian^4 at each grid point
        end
          grad_Si=((1-epsilon)*term1+term2+2*term3+term4)*dt;      % change
in Si after time dt
      Si=Si_old+grad_Si; % Si at time t+dt
            if(rem(i,1000*dt)==0)
      figure(f2)
       plot(x,Si) % Plotting Si after 1000dt
          axis([0 40 -1 1])
       title(['Time=' num2str(i)]);
             pause(0.0001)
            end
      end
```

Matlab code solving PFC using **Fourier Transform**

```
      x=0:dr:80; % grid size
      dr=0.5;
       Si(1:((length(x)+1)/2))=0;             % Initializing Phase variable
Si to left of mid region in grid
        Si(((length(x)+1)/2)+1)=0.2;          % Initializing Phase variable
Si at mid value in space
        Si(((length(x)+1)/2)+2:length(x))=0;  % Initializing Phase variable
Si to right of mid value in grid

      Si_3=Si.^3;       % Calculating non linear Si^3.
      N=length(x);
      delta_k=(2*pi)/(N*(dr));  % Discretization of Space variable k
       z=[-N/2+1:1:0 0:1:N/2];
      k_x=delta_k*z;          % Vector k in fourier space
      y1=(fft(Si,length(k_x)));    % Calculating fast fourier transform of
Phase variable Si
      y2=(fft(Si_3,length(k_x)));  % Calculating fast fourier transform of
Phase variable Si^3
      Si_f=(y1);
      Si_3f=(y2);

      t=35;
      dt=0.0001;
      epsilon=0.7; % Setting PFC parameter Si
      f1=figure;
      plot(x,(Si));   % Plotting initial Si at time=0
      title('Time = 0');
       f2=figure;
      for cnt=0:dt:t
          for cnt1=1:length(Si_f)
                  cnt2=cnt1;
```

```
            term1(cnt1)=(-((k_x(cnt2))^2)*(-epsilon+(1-
(k_x(cnt2))^2)^2))*dt;   % Converting PFC equation of motion differential
equation as per fourier transformation

      grad_Si_f(cnt1)=Si_f(cnt2)*exp((term1(cnt1)));     %     calculating
gradient of fourier of Si.
      grad_Si_3f(cnt1)=(-(Si_3f(cnt2))*(((k_x(cnt2))^2))*dt);            %
calculating gradient of fourier of Si^3.
          end

      Si_f=(grad_Si_f+grad_Si_3f); % Si in fourier space at t+dt
      Si=(ifft(Si_f,length(k_x))); % Taking Si back to real space

       Si_3=Si.^3;  % Updating Si^3 from new Si
       Si_3f=(fft(Si_3,length(k_x)));  % Updating fourier transform of  Si^3
      if(rem(cnt,1000*dt)==0)
      figure(f2)
           Si_new=Si((length(x)+1)/2:length(x));     %  Considering  phase
variable Si after 1000*dt
           x1=x((length(x)+1)/2):dr:x(length(x));
      plot(x1,Si_new)          % Ploting Si after 1000dt

      title(['Time' num2str(cnt)]);
        pause(0.0001)
      end
      end
```

REFERENCES

(1) Li, L.; Jahanian, P.; Mao, G. *J. Phys. Chem. C* **2014**, *118*, 18771–18782.

(2) Kahl, G.; Löwen, H. *J. Physics: Condens. Matter* **2009**, *21*.

(3) Neuhaus, T.; Härtel, A.; Marechal, M.; Schmiedeberg, M.; Löwen, H. *Eur. Phys. J. Spec. Top.* **2014**, *223*, 373–387.

(4) Cacciuto, A.; Auer, S.; Frenkel, D. *Nature* **2004**, *428*, 404–406.

(5) Emmerich, H.; Löwen, H.; Wittkowski, R.; Gruhn, T.; Tóth, G. I.; Tegze, G.; Gránásy, L. *Adv. Phys.* **2012**, *61*, 665–743.

(6) Ramakrishnan, T. V.; Yussouff, M. *Phys. Rev. B* **1979**, *19*, 2775–2794.

(7) Likos, C. N.; Mladek, B. M.; Gottwald, D.; Kahl, G. *J. Chem. Phys.* **2007**, *126*, 224502.

(8) Donev, A.; Vanden-Eijnden, E. *J. Chem. Phys.* **2014**, *140*, 234115.

(9) Smoluchowski, M. V. *Ann. Phys.* **1916**, *353*, 1103–1112.

(10) Podmaniczky, F.; GI Tóth, G. T., T. Pusztai…. *J. Cryst. Growth* **2016**.

(11) Tóth, G. I.; Tegze, G.; Pusztai, T.; Tóth, G.; Gránásy, L. *J. Physics: Condens. Matter* **2010**, *22*.

(12) Alster, E.; Elder, K. R.; Hoyt, J. J.; Voorhees, P. W. *Phys. Rev.* **2017**, *95*.

(13) Podmaniczky, F.; Tóth, G. I.; Tegze, G.; Gránásy, L. *Metall. Mater. Trans.* **2015**, *46*, 4908–4920.

(14) Ofori-Opoku, N.; Stolle, J.; Huang, Z.-F.; Provatas, N. *Phys. Rev. B* **2013**, *88*.

(15) Van Teeffelen, S.; Likos, C. N.; Löwen, H. *Phys. Rev. Lett.* **2008**, *100*.

(16) Van Teeffelen, S.; Backofen, R.; Voigt, A.; Löwen, H. *Phys. Rev.* **2009**, *79*.

(17) Tegze, G.; Gránásy, L.; Tóth, G. I.; Podmaniczky, F.; Jaatinen, A.; Ala-Nissila, T.; Pusztai, T. *Phys. Rev. Lett.* **2009**, *103*.

(18) Gránásy, L.; Podmaniczky, F.; Tóth, G. I.; Tegze, G.; Pusztai, T. *Chem. Soc. Rev.* **2014**, *43*, 2159–2173.

(19) Tóth, G. I.; Tegze, G.; Pusztai, T.; Gránásy, L. *Phys. Rev. Lett.* **2012**, *108*.

(20) Neuhaus, T.; Schmiedeberg, M.; Löwen, H. *Phys. Rev.* **2013**, *88*.

(21) Tegze, G.; Gránásy, L.; Tóth, G. I.; Douglas, J. F.; Pusztai, T. *Soft Matter* **2011**, *7*, 1789–1799.

(22) Wang, Q.; Keffer, D. J.; Nicholson, D. M.; Thomas, J. B. *Phys. Rev.* **2010**, *81*.

(23) Knepley, M. G.; Karpeev, D. A.; Davidovits, S.; Eisenberg, R. S.; Gillespie, D. *J. Chem. Phys.* **2010**, *132*, 124101.

(24) Gillespie, D.; Nonner, W.; Eisenberg, R. S. *Phys. Rev.* **2003**, *68*.

(25) Rosenfeld, Y. *J. Chem. Phys.* **1993**, *98*, 8126.

(26) Li, Z.; Wu, J. *Phys. Rev.* **2004**, *70*.

ABSTRACT

ENGINEERING CRYSTALLIZATION via PHASE FIELD CRYSTAL MODEL

Advisor: Dr. Korosh Torabi

Major : Material Science and Engineering

Degree: Master of Science

Charge transfer complex material demonstrate morphological transitions while electro-crystallized on a substrate electrode under varying solute concentration and applied overpotential. It is hypothesized that variations in these parameters affect the thermodynamics and the kinetics of the electro-crystallization process. Having analysed these results, we resort to applying phase field crystal(PFC) model for our theoretical study. Our initial literature review laid foundation to consider PFC model as a powerful tool to study various aspect of crystallization process. In a PFC model the thermodynamic state of a system under study is defined in terms of Helmholtz free energy functional of density profile $F = F[\rho(r)]$.Our numerical solution of the time-dependent PFC model demonstrates that the phase transition behaviour between a periodic crystal phase and a homogenous phase can be tuned by changing parameters within the PFC equation. These simulations also predicted the nature of the interface between solid/liquid phase at different simulation conditions. Moreover, it was evident from our results that solution of the PFC equation of motion through Fast Fourier Transform algorithm is computationally faster which facilitates the simulation of a large system.

Autobiographical Statement

Following my deep interest in the field of Material science and Engineering I was motivated to pursue my master's studies in this major at Wayne State University, Detroit United States. It was during the initial phase of regular coursework in this major I was introduced to the tool of modelling and simulation applied to various area of research. In particular I was deeply impressed with the concepts of statistical mechanics and advanced thermodynamics applied to research problems at microscopic level. On realizing my new found interest in the application of Modelling and Simulation techniques to fundamental research topic, I choose to work under the supervision Dr Korosh Torabi, Asst Prof Department of Chemical and Material science Engineering at Wayne State University for my Masters degree thesis work. I was fortunate to have reached out to him at a time when he had just started working on a collaborated research work with Dr Guangzhao Mao experimental group on a project outlined as the "Engineering the morphology of electro crystallization kinetics of organic nanorods on a substrate ".On Dr Torabi recommendation I was lean towards undertaking this research via experimental and theoretical route. The experimental part of my research work involves electrocrystallization of charge transfer complex TTFBr nanorods on a selectively oriented substrate followed up by morphological analysis via Atomic force microscopy imaging. Moreover, on the theoretical front I am involved in investigating previous literature work conducted via utilizing Phase field crystal thermodynamic model derived from the concepts of Classical density functional theory towards studying phase transition of materials on a substrate. On a final note I once again wants to give my sincere regards to Dr Torabi for his immense support and valuable guidance in letting me explore and build my foundation in areas from the point of view of statistical mechanics and Classical Thermodynamics.